STATE OF CALIFORNIA • DEPARTMENT OF TRANSPORTATION

TECHNICAL REPORT DOCUMENTATION PAGE

TR0003 (REV 10/98)

ADA Notice

For individuals with sensory disabilities, this document is available in alternate formats. For information call (916) 654-6410 or TDD (916) 654-3880 or write Records and Forms Management, 1120 N Street, MS-89, Sacramento, CA 95814.

1. REPORT NUMBER	2. GOVERNMENT ASSOCIATION NUMBER	3. RECIPIENT'S CATALOG NUMBER
CA22-3985		

4. TITLE AND SUBTITLE

Liquefaction Effects and a Probabilistic CPT-Based Liquefaction Ground Settlement Procedure

5. REPORT DATE

09/16/2022

6. PERFORMING ORGANIZATION CODE

7. AUTHOR

Jonathan D. Bray, Franklin R. Olaya

8. PERFORMING ORGANIZATION REPORT NO.

UCB/GT 2022-04

9. PERFORMING ORGANIZATION NAME AND ADDRESS

University of California, Berkeley
1608 4th Street, Suite 220
Berkeley, CA 95816

10. WORK UNIT NUMBER

11. CONTRACT OR GRANT NUMBER

65A0774 TO 005

12. SPONSORING AGENCY AND ADDRESS

California Department of Transportation (Caltrans)
1727 30th Street, MS-83, Sacramento, CA 95816

13. TYPE OF REPORT AND PERIOD COVERED

Final Report

14. SPONSORING AGENCY CODE

15. SUPPLEMENTARY NOTES

Supplemental Report: CPT CASE HISTORIES OF POST-LIQUEFACTION FREE-FIELD GROUND SETTLEMENT, dated July 11, 2022; Report No. UCB/GT 2022-02; Number of Pages: 25

16. ABSTRACT

Through examining field case histories, experiments, and analyses insights are shared on the effects of liquefaction. The problem of liquefaction-induced settlement is best viewed by examining soil response at the element level and soil deposit performance through its system response. The state, cyclic responses, and post-liquefaction volumetric strain of uniform clean sand, sandy gravel, nonplastic silty sand, and nonplastic silt can be captured in a unified manner using relative density or the state parameter. The system response of a soil deposit often governs the consequences of liquefaction triggering, including the formation of ejecta. Effective stress analysis and a CPT-based method employing the liquefaction ejecta demand parameter can be used to evaluate system response and provide a rough estimate of ejecta-induced structural settlement. The CPT and cyclic tests provide complementary insights. However, the depositional environment should be also characterized because geologic details, such as soil fabric, are important in evaluating liquefaction effects. Detailed logging of high-quality continuous samples can be used to examine soil fabric. A probabilistic CPT-based post-liquefaction ground settlement procedure is proposed that utilizes laboratory and field case history databases. Correlations are developed to estimate Dr or ψo to enable use of the volumetric strain models. Calibration and adjustment factors enable the proposed model to capture the observed post-liquefaction ground settlement.

17. KEY WORDS	18. DISTRIBUTION STATEMENT	
Liquefaction case histories, liquefaction-induced settlement, post-liquefaction settlement, liquefaction triggering, CPT, structural settlement, liquefaction effects, ground settlement		
19. SECURITY CLASSIFICATION *(of this report)*	**20. NUMBER OF PAGES**	**21. COST OF REPORT CHARGED**
	43	

DISCLAIMER STATEMENT

This document is disseminated in the interest of information exchange. The contents of this report reflect the views of the authors who are responsible for the facts and accuracy of the data presented herein. The contents do not necessarily reflect the official views or policies of the State of California or the Federal Highway Administration. This publication does not constitute a standard, specification, or regulation. This report does not constitute an endorsement by the Department of any product described herein.

For individuals with sensory disabilities, this document is available in alternate formats. For information, call (916) 654-8899, TTY 711, or write to California Department of Transportation, Division of Research, Innovation and System Information, MS-83, P.O. Box 942873, Sacramento, CA 94273-0001.

GEOYSTEMS ENGINEERING

Liquefaction Effects and a Probabilistic CPT-Based Liquefaction Ground Settlement Procedure

by

Jonathan D. Bray and Franklin R. Olaya

Report No. UCB/GT 2022-04

September 16, 2022

Department of Civil and Environmental Engineering
University of California
Berkeley, California

ABSTRACT

Through examining field case histories, experiments, and analyses insights are shared on the effects of liquefaction. The problem of liquefaction-induced settlement is best viewed by examining soil response at the element level and soil deposit performance through its system response. The state, cyclic responses, and post-liquefaction volumetric strain of uniform clean sand, sandy gravel, nonplastic silty sand, and nonplastic silt can be captured in a unified manner using relative density or the state parameter. The system response of a soil deposit often governs the consequences of liquefaction triggering, including the formation of ejecta. Effective stress analysis and a CPT-based method employing the liquefaction ejecta demand parameter can be used to evaluate system response and provide a rough estimate of ejecta-induced structural settlement. The CPT and cyclic tests provide complementary insights. However, the depositional environment should be also characterized because geologic details, such as soil fabric, are important in evaluating liquefaction effects. Detailed logging of high-quality continuous samples can be used to examine soil fabric. A probabilistic CPT-based post-liquefaction ground settlement procedure is proposed that utilizes laboratory and field case history databases. Correlations are developed to estimate D_r or ψ_o to enable use of the volumetric strain models. Calibration and adjustment factors enable the proposed model to capture the observed post-liquefaction ground settlement.

Acknowledgements

The numerous significant contributions of Professor H. Bolton Seed over his distinguished career are recognized, some of which are important components of the proposed procedure for estimating liquefaction-induced ground settlement. Prof. Kenji Ishihara also provided data, insights, and inspiration for this work. Zorana Mijic and Daniel Hutabarat of UC Berkeley shared data and insights of their Ph.D. research with us.

Support for this research was provided primarily by grants from the California Department of Transportation (Caltrans) through Agreement 65A0774 Amendment Number TO 005 and from the U.S. National Science Foundation (NSF) through CMMI-1956248. The findings, opinions, and conclusions presented in this report are those of the authors and do not necessarily reflect the views of the sponsors. The NSF-sponsored Geotechnical Extreme Events Reconnaissance (GEER) Association funding through grant CMMI-1266418 enabled researchers, including the first author, to document and learn from the case histories discussed in this report. Additionally, the College of Engineering at the University of California, Berkeley (UCB) provided support through the Faculty Chair in Earthquake Engineering Excellence.

We acknowledge the assistance of all NZ and US GEER team members who participated in post-earthquake reconnaissance and follow-on research relied upon in this study. Most importantly, we thank Misko Cubrinovski of the Univ. of Canterbury, who shared data and concepts freely. We also thank all those who participated in research that supported this study, including Michael Riemer, Rodolfo Sancio, Jennifer Donahue, Christine Beyzaei, Christopher Markham, Claudio Cappellaro, Sean Rees, Ribu Dhakal, Jorge Macedo, Roberto Luque, Josh Zupan, Mark Stringer, Merrick Taylor, Tom O'Rourke, Brendon Bradley, Sjoerd Van Ballegooy, Mike Jacka, Rick Wentz, Ian McCahon, Nick Traylen, and Iain Haycock. We also thank Uri Eliahu and Pedro Espinosa of ENGEO, Inc. for providing CPT data for Treasure Island, the team of engineers who worked on the Treasure Island project, which included Pedro Espinosa, Phil Stuecheli, Stefanos Papadopoulos, Joe Tootle, Uri Eliahu, Shah Vahdani, Bahareh Heidarzadeh, Steve Dickenson, Michael Beaty, Juan Pestana, Nick Sitar, Michael Riemer & Chris Markham, and R. Luna for providing CPT data for the Treasure Island. We thank J.P. Bardet for providing CPT data for the Marina District, and the U.S. Geologic Survey and the New Generation Liquefaction project for providing access to liquefaction reports and CPT data for the Marina District and Treasure Island. Norm Abrahamson of UC Berkeley assisted in the development of the probabilistic models. Ross Boulanger of UC Davis provided helpful feedback after discussing aspects of the work. Review comments by AnhDan Le and Sharon Yen of Caltrans were helpful.

Table of Contents

Chapter 1 INTRODUCTION

1.1 Research Motivation

The consequences of triggering soil liquefaction in a soil deposit can be negligible to severe. At the element level, the accumulation of shear strain beyond the volumetric threshold shear strain in a soil layer generates excess pore-water pressure that reduces effective stress (Dobry and Ladd 1980). The stiffness and strength of a soil element can degrade rapidly as its effective stress reduces to a low value. Understanding, characterizing, and modeling the cyclic response of a soil unit that is susceptible to liquefaction is crucial to evaluating the effects of liquefaction at a site. However, the system response of the entire soil deposit should also be evaluated to assess the effects of soil liquefaction at the site. For example, a site with a nearby free-face slope that imposes a significant static driving stress can undergo a damaging lateral spread if a continuous soil layer liquefies. Conversely, gently sloping ground with isolated soil units that liquefy may not displace because the liquefied soil units are not laterally continuous. At some level ground sites, the formation of sediment ejecta produces extensive ground cracking and the loss of foundation support, which damages infrastructure. At other level ground sites, earthquake shaking triggers soil liquefaction in a deep soil layer that is well below structure foundations so that damaging shear-induced displacement does not develop. In these cases, the dissipation of the excess pore-water pressure in the soil can still produce ground settlement due to sedimentation and reconsolidation volumetric strain processes; however, the ground settlement may be uniform and moderate, so it causes no infrastructure damage.

Performance-based engineering requires robust methods to evaluate liquefaction effects. Nonlinear dynamic soil structure interaction (SSI) effective stress analyses can provide key insights as well as reasonable estimates of liquefaction-induced ground and structure movements. Nonlinear effective stress analysis can capture the element response of soil and the system response of the soil deposit, if performed with sound soil constitutive models that are properly calibrated and validated to capture the element response of soil and employed in numerical models that capture system response features (e.g., seismic site response, soil layering, and water flow). Alternatively, empirical procedures may be used in engineering practice because they can be calibrated to estimate reliably the observed ground and structure performance. Researchers have developed empirical procedures to estimate liquefaction-induced ground settlement and lateral movement using field case history data with models informed by laboratory test results and mechanics. In these methods, the complex processes involved in liquefaction triggering and its consequences are captured using proxies that represent the state of the soil and the seismic demand. For example, cone penetration test (CPT)-based empirical methods for estimating liquefaction-induced level ground settlement and sloping ground lateral spread displacement methods are widely used in engineering practice (e.g., Zhang et al. 2002, 2004). There is merit to developing alternative methods, especially if the empirical methods are informed by new field case histories that explore the response of a wider range of soil types and seismic demands.

In this report, soil liquefaction effects of level ground sites composed of sand, sandy gravel, silty sand, nonplastic silt, and slightly plastic clayey silt with and without structures are explored. The element and system responses of the individual soil layers and the soil deposits they form are examined. Soil system responses are investigated to characterize the severity of soil ejecta so its effects on infrastructure can be assessed. A probabilistic CPT-based procedure for estimating post-liquefaction ground settlement is presented. Recommendations for its use in engineering practice are shared.

1.2 Liquefaction-Induced Movements

Liquefaction has the potential to damage infrastructure (e.g., bridges and buildings). The bearing

capacity failure of buildings, such as the 5-story building in Adapazai, Turkey shown in Figure 1.1a, the settlement and lateral displacement of another building in Adapazari shown in Figure 1.1b, and the ejecta-induced settlement of a 2-story building in Christchurch, New Zealand shown in Figure 1.1c illustrate some of the direct consequences of liquefaction on structures with shallow foundations (Bray et al. 2004, 2014a). The fire shown in Figure 1.1d that consumed part of Kobe, Japan reminds engineers of indirect consequences of liquefaction that can devastate a city (Akai et al. 1995). In numerous other post-earthquake photographs (not shown), there is no discernable damage to structures even though current procedures indicate the factor of safety against liquefaction triggering (FS_L) is well less than one (e.g., Beyzaei et al. 2018b). Thus, the effects of liquefaction on structures can be negligible to severe.

Several of the key mechanisms of liquefaction-induced settlement are illustrated in Figure 1.2. They can be categorized as shear-induced, volumetric-induced, or ejecta-induced deformation and estimated separately as recommended by Bray and Macedo (2017). Alternatively, the mechanisms can be combined in estimating liquefaction-induced settlement as recommended by Bullock et al. (2019). The former approach is employed in this study to examine the contribution of each component of settlement. Ejecta are not produced in some cases (i.e., thick nonliquefiable crust overlying a thin liquefied soil layer) and it is severe in other cases, so there is merit to separating it from the other two mechanisms. Moreover, the shear-induced component of settlement governs in some cases, and in other cases when the liquefiable layer is deep, it is negligible. Lastly, uniform volumetric-induced ground settlement contributes to total settlement of infrastructure without tilt, whereas differential volumetric-induced ground settlement contributes to differential settlement and tilt. Bray and Macedo (2017) proposed a CPT-based probabilistic method to estimate shear-induced liquefaction building settlement. Hutabarat and Bray (2022) proposed a CPT-based method to categorize liquefaction ejecta severity which is used in this report to develop a rough estimate of this component of settlement. A probabilistic CPT-based method to estimate volumetric-induced ground settlement is proposed in this report. Before discussing the proposed procedure, it is useful to summarize some of the key aspects of soil liquefaction at the element and system response levels.

1.3 Report Organization

The remaining parts of this report are organized into six chapters as follows:

- Chapter 2 discusses the liquefaction of soil at the element level. Liquefaction of sand, nonplastic silty soils and clayey silts are examined using cyclic test results of soils with different gradations and varying plasticity. The initial state of uniform nonplastic soils can be successfully characterized with the relative density and the state parameter.

- Chapter 3 examines the system response of soil deposits containing liquefiable layers. Effective stress analyses of thick clean sand deposits and stratified silty soil deposits are presented to this end. These analyses confirm the soil layer stratification, vertical hydraulic conductivity profile, and depth of liquefaction triggering largely determine if ejecta will or will not be produced if strongly shaken. A CPT-based ejecta severity procedure which uses liquefaction ejecta demand (L_D) and crust layer resistance (C_R) parameters is summarized. L_D and C_R are further used to provide rough estimates of ejecta-induced settlement.

- Chapter 4 discusses the role of depositional environment on liquefaction triggering and its manifestations. The benefits of high-quality soil sampling and cyclic testing of key soil units are highlighted. Scanning electron microscope imagery is useful to identify soil characteristics such as soil fabric, cementation, and particle shape. An illustrative example showing the effectiveness of different site characterization tools is presented.

- Chapter 5 summarizes the mechanisms of post-liquefaction volumetric strain and maximum shear strain development. A family of strain potential models are presented using a comprehensive database of post-liquefaction laboratory test results. A relationship between the factor of safety against liquefaction and the volumetric strain potential is presented. The development of a comprehensive database of post-liquefaction ground settlement field case histories is presented.

- Chapter 6 presents a probabilistic CPT-based liquefaction ground settlement procedure that is based on the findings, functional models and databases discussed in Chapter 5. Illustrative examples of the application of the procedure are provided.

- Chapter 7 summarizes the main conclusions and findings of this report.

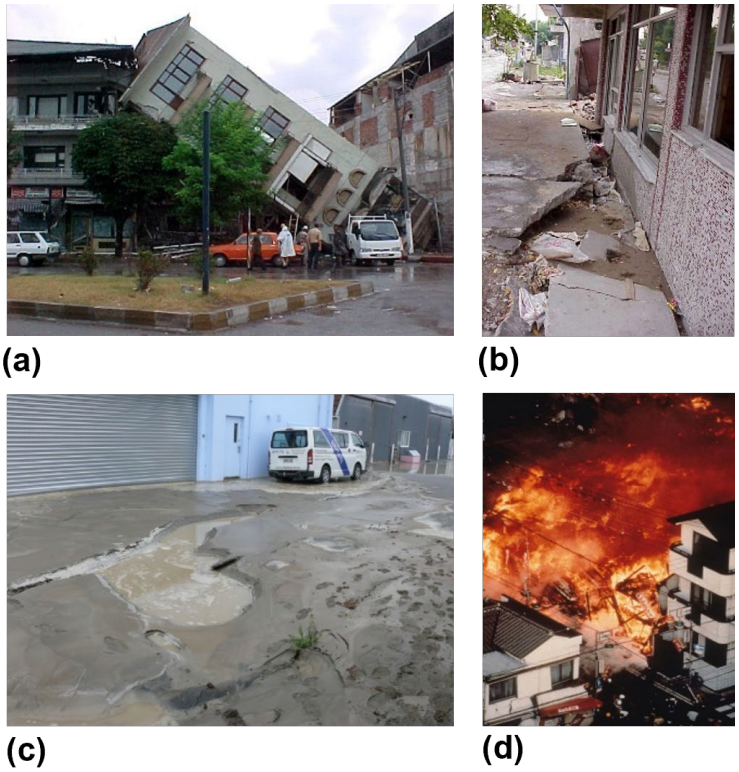

Figure 1.1 Buildings damaged by liquefaction: (a) overturned 5-story building in Adapazari, (b) laterally displaced and settled building in Adapazari, (c) ejecta affecting building in Christchurch, and (d) fire in Kobe (Bray et al. 2004, 2014a, Akai et al. 1995).

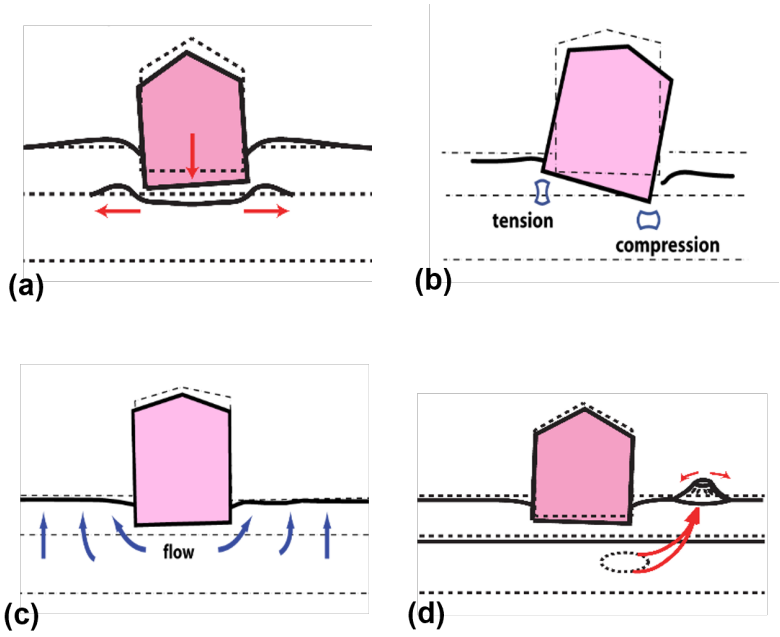

Figure 1.2. Liquefaction-induced structure displacement mechanisms: (a) shear-induced punching failure, (b) shear-induced SSI ratcheting, (c) volumetric-induced reconsolidation settlement, and (d) ejecta-induced ground loss.

Chapter 2 SOIL LIQUEFACTION AT THE ELEMENT LEVEL

2.1 Clean Uniform Sand

Much of the profession's understanding of soil liquefaction is based on laboratory experiments and field case histories involving clean uniform sand. For example, the Boulanger and Idriss (2016) empirical CPT-based liquefaction triggering procedure is largely based on sites with relatively thick deposits of clean sand or silty sand with fines contents (FC) ≤ 35%. Fewer than 14% of their case histories contain critical layers with FC > 35%. Experiments that shape our concepts have been predominantly conducted on laboratory-prepared specimens of clean sand (e.g., Seed 1979). Silty soils have been tested less frequently (e.g., Bray and Sancio 2006). Even well-graded clean sands have been tested less frequently than uniform clean sand. The reference material for many of our liquefaction assessment methods are clean uniform sand and the state of well-graded sand, silty sand, and silt is adjusted to reflect that of a uniform clean sand with equivalent cyclic responses (i.e., through a clean sand equivalent penetration resistance, such as the CPT q_{c1ncs}, Boulanger and Idriss 2016). There is an implicit assumption in the application of empirically based liquefaction procedures and concepts to a wide range of soils that they can be adjusted to capture adequately the cyclic response and performance of soils other than clean uniform sand. Research investigating the validity of this assumption is limited, which contributes to uncertainty in applying uniform clean sand methods to other soil types (Bray et al. 2017).

2.2 Relative Density and State Parameter

Relative density (D_r) is used to characterize the state of clean sand. Cubrinovski and Ishihara (2002) found the Japanese Standard JIS A 1224:2009 Test Method yielded consistent maximum void ratio (e_{max}) and minimum void ratio (e_{min}) values for silty sand with nonplastic FC up to 35% for a comprehensive database with over 300 native soils. Reexamination of their database found reasonable e_{max} and e_{min} values were also obtained for nonplastic soils with even higher FC (Mijic et al. 2021a). Recently, Mijic et al. (2021a) obtained consistent e_{max} and e_{min} values for Christchurch relatively uniform nonplastic silty sand and sandy silt with FC ≤ 70%, and the e_{max} and e_{min} values of nonplastic silt with FC = 100% were only slightly inconsistent. Tests on a wide range of uniform nonplastic soil indicate e_{max} decreases slightly initially with increasing FC from 0% to about 30% and then increases with a higher rate of increase with increasing FC > 30%, and e_{min} tends to decrease with increasing FC from 0% to about 30-40% and increases slightly from approximately 40% to 100% fines (e.g., Cubrinovski and Ishihara 2002, Thevanayagam et al. 2002, and Mijic et al. 2021a). Thus, $FC \approx 30\%$ is the approximate threshold for a fines-dominated particle structure for many silty sands. The use of D_r with e_{max} and e_{min} measured in a consistent manner enables the responses of uniformly graded nonplastic sand, silty sand, and silt at the same state to be compared. Soil can also be characterized with the initial state parameter (ψ_o) defined as.

$$\psi_o = (e_o - e_c)|_{p'_o} \tag{1}$$

where e_o is the current void ratio at its current mean effective stress, p'_o, and e_c is the void ratio at the critical state at the same p'_o (Been and Jefferies 1985). The initial state parameter is useful to describe the response of many soil types over a wide range of stress levels and loading conditions. It captures the key influences of soil density and effective confining stress, as well as other factors such as soil compressibility, grain size, and grain shape, and thus is more informative than D_r. Jefferies and Been (2016) found the important threshold between contractive and dilative responses to be ψ_o = -0.05 for simple shear conditions. Shuttle and Cunning (2007, 2008) identified ψ_o = -0.05 as a general threshold

between contractive and dilative responses, and Robertson (2016) and Mayne and Styler (2018) also use ψ_o = -0.05 as the contractive/dilative response threshold in the field.

2.3 Nonplastic Silty Soil Liquefaction

Polito and Martin (2001), Bray and Sancio (2006), Beyzaei et al. (2018b), Markham et al. (2018), Mijic et al. (2021b), and other researchers have shown that nonplastic silty soils liquefy in a manner like many clean sands. They often exhibit a cyclic mobility response due in part to the angularity of many silt-size particles. As an example, the representative responses of three cyclic simple shear (CSS) 16-mm thick test specimens composed of relatively homogeneous high-quality samples of different natural soil units in Christchurch are shown in Figure 2.1 (Mijic et al. 2021b). The Unified Soil Classification System (USCS) classifications for these soils are uniform sand (SP) with *FC* = 2%, silty sand (SM) with nonplastic *FC* = 44%, and silt (ML) with nonplastic *FC* = 64% with their grain size distributions shown in Figure 2.2a and their particle shapes shown in Figure 2.2b. These soils are of uniform gradation and composed of angular particles. The SP, SM, and ML test specimens have similar D_r values of 88%, 80%, and 82% and similar ψ_o values of -0.13, -0.11, and -0.07, respectively, and they were tested with similar cyclic stress ratios (*CSR*) of 0.16 to 0.22. Their cyclic responses are similar in terms of shear stress vs. shear strain and the development of excess pore-water pressure as indicated by the changes in the normalized vertical effective stress (σ'_v / σ'_{vo}).

The finer fraction of a nonplastic silty sand controls particle fabric and the response of soils with *FC* greater than about 30% (Cubrinovski and Ishihara 2002 and Thevanayagam et al. 2002). Therefore, a nonplastic silty sand with *FC* > 30% should respond like a nonplastic silt, which is confirmed by the comparison of the SM and ML material responses shown in Figure 2.1b and 2.1c. Moreover, the cyclic response of a uniform fine sand should not differ appreciably from that of a uniform coarse nonplastic silt if their mineralogy, particle shape, etc. are the same, and by inference, it should not differ appreciably from a nonplastic uniform silty sand. Fines content does not discriminate the mechanical responses of uniform soils of the same mineralogy and particle shape for these cases because little fundamentally changes as a uniform grain size distribution translates horizontally across the #200 sieve threshold. A particle size threshold of 0.075 mm does not separate fundamentally different soil responses to monotonic or cyclic loading. Mineralogy, particle shape, etc. are more important in determining the cyclic responses of uniform fine sand and uniform coarse silt.

Cubrinovski and Ishihara (2000) and Jefferies and Been (2016) showed, however, with all other conditions maintained, nonplastic fines increased a sand's compressibility, which reduces its penetration resistance significantly and also reduces its cyclic resistance ratio (*CRR*). The soils they investigated were typically well-graded. Fines content is more informative for well-graded soils. Changes in the tail of the grain size distribution curve reflect changes in soil compressibility which in turn affects *CRR*, though fines content affects penetration resistance more than *CRR*.

2.4 Clayey Silt Liquefaction

Extensive liquefaction of clayey silt in Adapazari during the 1999 Kocaeli earthquake led to research that developed the Bray and Sancio (2006) plasticity index (*PI*) ≤ 12 and water content-to-liquid limit ratio (*w/LL*) ≥ 0.85 criteria for the liquefaction susceptibility of fine-grained soil. Their initial hypothesis was liquefaction susceptibility would reduce systematically as *PI* increased, but they could not discern significant changes in the cyclic responses of the natural clayey silt soils in the results of over a hundred cyclic triaxial tests of high-quality samples of natural soils. Their *PI* ≤ 12 criterion is similar to the finding of Ishihara (1993) that fine-grained soils with *PI* ≤ 10 do not differ in their *CRR*, whereas *CRR* increases systematically as *PI* increases in soils with *PI* > 10. The Idriss and Boulanger (2008) *PI* < 7 liquefaction susceptibility criterion is sometimes compared with the Bray and Sancio *PI* ≤ 12 criterion, but a direct comparison of these criteria is inappropriate because they use different definitions of liquefaction. Idriss and Boulanger (2008) reserve the term liquefaction in the use of their criterion to soils that can be evaluated using penetration resistance (e.g., CPT tip resistance); whereas Bray and Sancio

(2006) use the term liquefaction for fine-grained soils if their stress-strain responses in cyclic tests are like the stress-strain response of clean sand that are classified as liquefiable. Bray and Sancio (2008) and Boulanger and Idriss (2008) agree clayey silt soil can be sampled effectively, and therefore, laboratory testing should be used to characterize the cyclic response of these soils so that the consequences of their responses can be evaluated.

Although the Bray and Sancio (2006) test specimens used to develop their liquefaction susceptibility criteria were relatively homogenous, they possessed some variability as natural soil deposits. Donahue et al. (2007) prepared more homogeneous CSS test specimens by reconstituting them from mixtures of Adapazari silt and clay to explore this issue further. Representative test results of the first load cycle and load cycle to reach 5% shear strain are shown in Figure 2.3. The cyclic responses of the test specimens with *PI* = 2, 7, 10, and 11 are similar, and hence, should be considered similarly in terms of their cyclic responses in performance-based engineering assessments. The *PI* =14 test specimen displays "clay-like" behavior that differs noticeably from the lower *PI* test specimens shown in Figure 2.3. In another study, Beyzaei et al. (2018b) tested several Christchurch soils that included clean sand, nonplastic silt, and *PI* = 10 silts whose test results are shown in Figure 2.4. The cyclic responses of the uniform fine clean sand and the *PI* =10 silt test specimens are nearly identical with the nonplastic silt deviating only slightly from their responses, though in part because a higher *CSR* was applied to it. Thus, it is prudent to characterize the cyclic response of clayey silts (whether eventually termed liquefaction or cyclic failure) through a program of laboratory testing that includes consolidation tests, monotonic tests, and cyclic tests performed on high-quality retrieved natural soil test specimens.

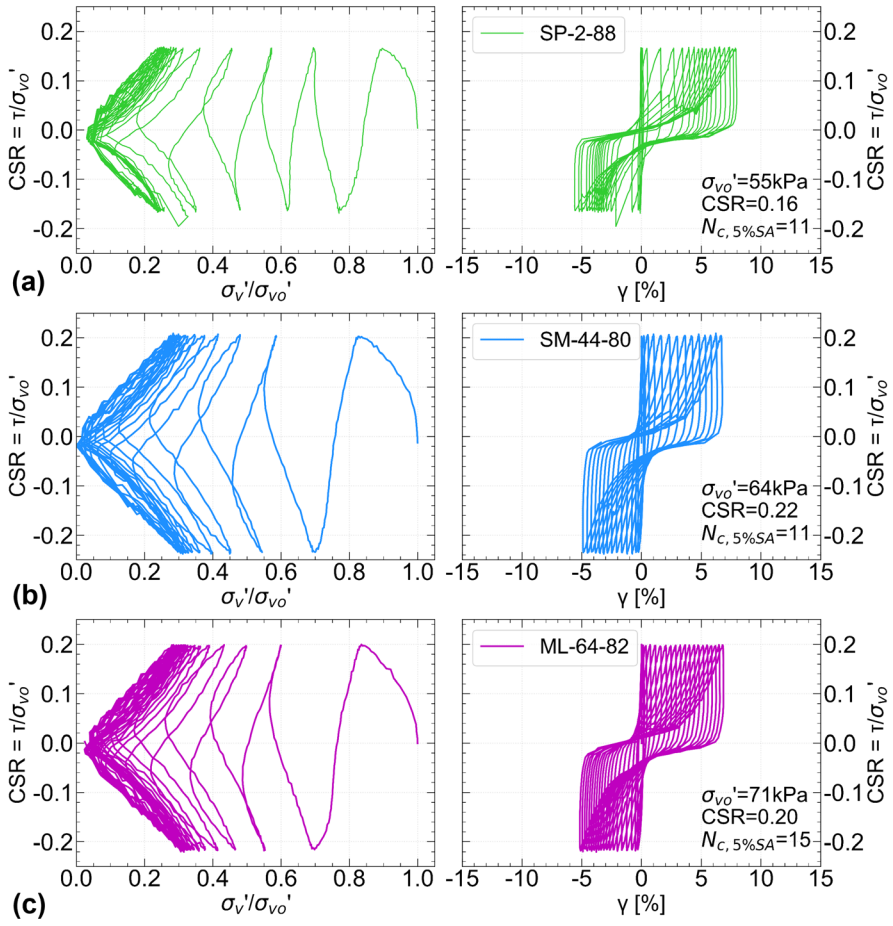

Figure 2.1. Cyclic simple shear response of test specimens: (a) SP-2-88, (b) SM-44-80, and (c) ML-64-82, where designation is USCS-*FC*-D_r (data from Mijic et al. 2021).

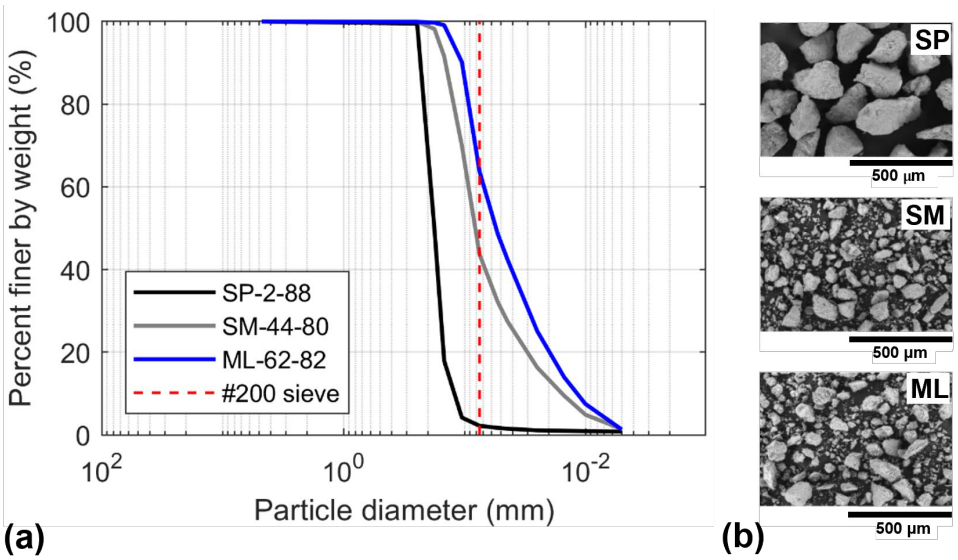

Figure 2.2. (a) Grain size distributions of sand, silty sand, and silt tested in southwest Christchurch with (b) SEM images of the soil particles (data from Mijic et al. 2021).

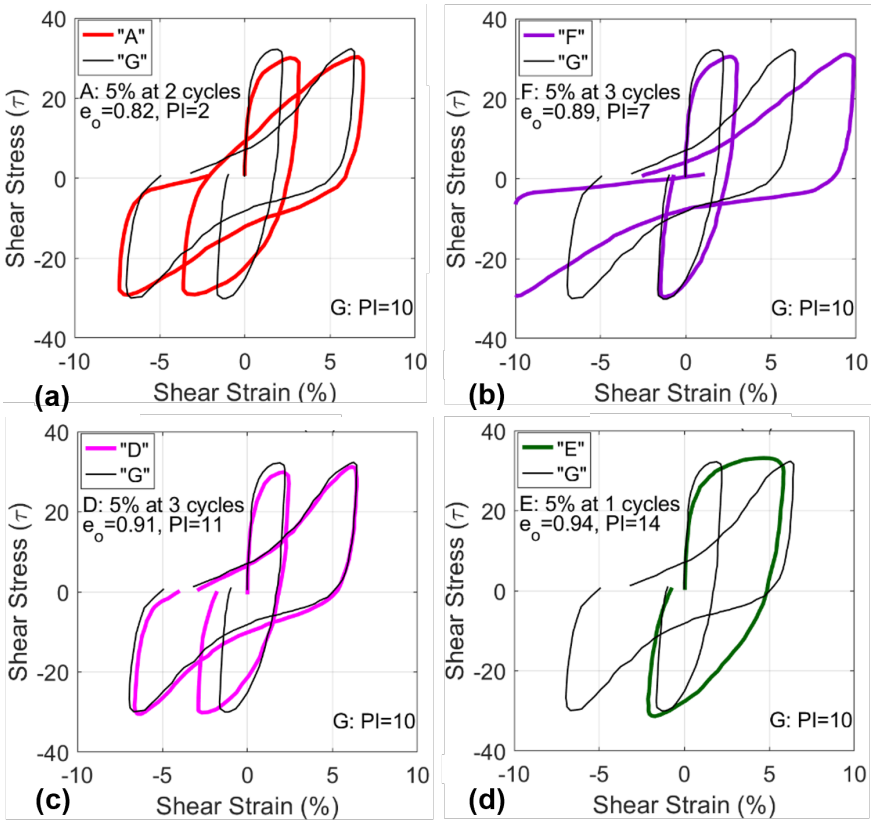

Figure 2.3. Cyclic Simple Shear Results: First Cycle and Cycle to reach 5% Shear Strain are compared to Soil "G". Soil "G" reaches 5% Shear Strain at 7 cycles, e = 0.68, $\sigma'_v \approx 137$ kPa, CSR = 0.21 (data from Donahue et al. 2007).

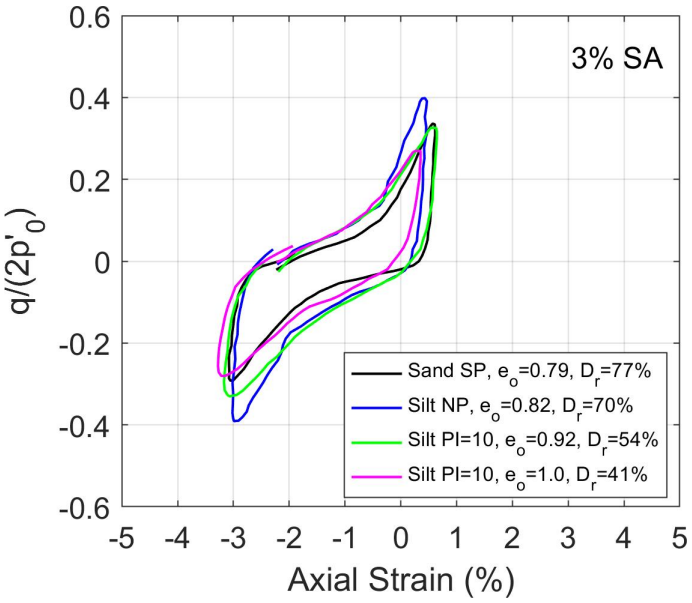

Figure 2.4. Stress-strain response for 3% single-amplitude (SA) axial strain; specimens reach 3% SA at 5 cycles, 4 cycles, 5 cycles, and 9 cycles for sand(EQC4-DM1B-7U-A), nonplastic silt(S21-DM1-3U-A), *PI*=10 silt (S33-DM1-8U-A), and *PI*=0 silt(S33-DM1-8U-B), respectively (data from Beyzaei et al. 2020).

Chapter 3 SYSTEM RESPONSE OF SOIL DEPOSITS CONTAINING LIQUEFIABLE Soils

3.1 System Response Factors

Although soil composed of angular nonplastic silt particles or low-plasticity clayey silt can liquefy in terms of developing high excess pore-water pressure and shear strain, the effects of liquefaction can differ greatly from those of loose clean sand. For example, the vertical hydraulic conductivity (k_v) of a soil unit plays an integral role in movement of water during and after earthquake shaking. The fine sand, nonplastic silty sand, nonplastic silt, and plastic silt tested by Beyzaei et al. (2018b) have $k_v \approx 10^{-2}$ cm/s, 10^{-3} cm/s, 10^{-4}-10^{-5} cm/s, and $<10^{-6}$ cm/s, respectively. The wide range of hydraulic conductivities of these soil units in stratified soil deposits will greatly affect the vertical flow of water in the soil deposit and hence its system response.

Several researchers have explored various aspects of the system response of soil deposits during earthquake shaking. Cubrinovski et al. (2018a) identified several key factors affecting the development of and consequences of liquefaction. The manifestation of liquefaction at the surface of free-field, level ground sites depends primarily on the thickness and vertical continuity of critical layers and other liquefiable materials in the deposit. Sites with thick zones of liquefiable soils in the top 10 m tend to produce ejecta and interbedded deposits of liquefiable and nonliquefiable soil layers do not.

Figure 3.1 illustrates the important role of soil deposit stratification in the formation of ejecta. CPT profiles of tip resistance (q_c) and soil behavior type index (I_c) at free-field Christchurch sites that produced ejecta are shown with red traces and sites without ejecta are shown with blue traces (Beyzaei et al. 2018a). The influence of peak ground acceleration (PGA) is shown by binning the CPT profiles by median estimated PGA_{M6} scaled to moment magnitude (M_w) = 6.0 (Beyzaei et al. 2018a). When $0.2\ g < PGA_{M6} < 0.4\ g$, sites with ejecta had thick layers of clean sand with I_c consistently less than 1.8, whereas sites without ejecta had highly stratified silt/sand deposits as indicated by highly variable I_c profiles. Many of the stratified soil sites shown in Figure 3.1 without surface manifestations of liquefaction (i.e., no ejecta) are cases in which liquefaction triggering procedures indicate liquefaction should have occurred. Cyclic triaxial (CTX) tests indicate many of the soil units at these sites liquefied at the element level at these intensity levels (Beyzaei et al. 2018b). However, they did not manifest liquefaction at the ground surface (i.e., produce ejecta) because low hydraulic conductivity silty soil layers resisted the vertical movement of water up through the soil profile. When $PGA_{M6} > 0.4\ g$, more stratified silt/sand deposits produced ejecta indicating the likelihood of ejecta increases for stratified soil sites at intense shaking levels. Sites with heavy buildings can also produce ejecta at lower levels of shaking due to SSI effects (Bray et al. 2004, Bray and Macedo 2017).

Effective stress analysis of thick clean sand deposits and stratified silty soil deposits by Hutabarat and Bray (2021a,b) confirm the post-shaking hydraulic characteristics of the soil profiles (i.e., soil layer stratification, vertical hydraulic conductivity profile, and depth of liquefaction triggering) largely determine if ejecta will or will not be produced if strongly shaken. Representative thick clean sand and stratified silty soil deposits in Christchurch are shown in Figure 3.2. The Ti Rakau site (Figure 3.2a) has a thick deposit of liquefiable clean sand-like material (Robertson 2016, modified soil behavior type index, $I_B > 32$) beneath a nonliquefiable crust. Parts of the thick clean sand unit liquefied and other parts of it generated high excess water pressures during the 2011 Christchurch and June earthquakes and produced severe ejecta (Hutabarat and Bray 2021b). As shown in Figure 3.3 liquefaction of a high k_v sand unit whose high excess water pressure are sustained by upward seepage from deeper hydraulically-connected high k_v sand units produce excess hydraulic head greater than that required for artesian flow, which results in ejecta manifesting at the ground surface. Conversely, the highly stratified Gainsborough site (Figure

3.2 b) produced no ejecta during the Canterbury earthquakes, even though it was shaken intensely by the 2010 Darfield, 2011 Christchurch, and 2011 June earthquakes. Effective stress analyses calibrated by established field and laboratory test methods indicate some soil layers at the Gainsborough site liquefied and other layers developed significant excess pore-water pressure, but they were relatively thin and isolated. High excess pore-water pressures did not develop over a thick zone directly beneath the nonliquefiable crust, and the excess hydraulic head (h_{exc}) never exceeded that required for artesian flow (h_A).

Effective stress analysis can reveal key system response characteristics that dictate the effects of liquefaction at a site (e.g., Cubrinovski et al. 2018a, and Hutabarat and Bray 2021a,b). The occurrence of sediment ejecta and its severity depend significantly on hydraulic processes after strong ground shaking ceases, which the simplified liquefaction triggering procedures do not consider. The Artesian Flow Potential (AFP) parameter (Hutabarat and Bray 2021a), which can be calculated in effective stress analysis (it depends on the size of the red zone shown in Figure 3.3b), captures the seismic demand and importantly, the hydraulic demand generated during and after earthquake shaking. The integration of AFP with time over a period of 180 s after the start of ground shaking produces the Ejecta Potential Index (EPI). Hutabarat and Bray (2021b) showed EPI captures the advection processes that govern the amount of upward seepage-induced artesian flow that determines ejecta severity. Sites with severe ejecta have high EPI values, and sites without ejecta have low EPI values. Although effective stress analysis of the seismic response of a liquefiable site provides great insight, it may be infeasible to perform advanced analysis for projects with limited subsurface data and ground motion recordings. Thus, the development of a reliable CPT-based procedure that does not require effective stress analysis has merit

3.2 CPT-Based Ejecta Severity Procedure

The Hutabarat and Bray (2022) CPT-based liquefaction ejecta assessment procedure employs two governing parameters: liquefaction ejecta demand (L_D) and crust layer resistance (C_R). The L_D parameter considers the excess hydraulic head (h_{exc}) and artesian water pressure that can develop at a site, and the C_R parameter considers the thickness of the nonliquefiable crust layer and its equivalent shear strength which suppresses manifestations of liquefaction. L_D is estimated as

$$L_D\ (\text{kN/m}) = \int_{z_A}^{z_B} \frac{k_{cs}}{k_v} (h_{exc} - h_A)\, dz \quad \text{when } h_{exc} \geq h_A; \quad 0, \text{ otherwise} \tag{2}$$

where z_A = depth from the ground surface to the top of the shallowest soil layer below the groundwater level with $I_c < 2.6$ that is at least 250-mm thick; z_B = depth from the ground surface to the top of the shallowest soil layer between the depths of z_A and 15 m with $I_c \geq 2.6$ that is at least 250-mm thick; and k_{cs} = baseline vertical hydraulic conductivity of clean sand with $I_c = 1.8$ (with k_v estimated using the Robertson and Cabal 2015 correlation). A soil layer's k_v directly influences the upward flow of water in a soil column that can induce post-shaking secondary liquefaction at shallow depths which generates ejecta. The water flowing upward from a deep liquefied layer can increase the h_{exc} in a shallow layer if the intermediate soil layers have high k_v values. Conversely, a low-k_v intermediate depth soil layer with sufficient thickness can restrict the upward flow of water from deep liquefiable layers. To capture this effect the normalized-k_v weighting factor ($\frac{k_v}{k_{cs}}$) is employed so a low permeability layer decreases L_D and a high permeability layer increases L_D. The thickness of the first continuous sand-like soil layer that liquefies beneath the nonliquefiable crust (z_{AB}) is also an indicator of the potential to generate sufficient artesian flow to produce ejecta. In the comparison of the two sites shown previously in Figure 3.2, the parameter z_{AB} at the Ti Rakau site (Figure 3.2a) is over 13 m thick, whereas it is less than 1 m thick at the Gainsborough site.

The other parameter C_R is estimated as

$$CC_{RR}\,(\text{kN/m}) = \int_0^{zz_A} ss_{uu}\,dddd \quad \text{where} \quad ss_{uu} = KK_{oo}\,\sigma'_{vvoo}\tan(\phi\phi_{cccc}),\ \text{if } II_{BB} > 22 \quad ss_{uu} = \frac{(qq_{tt} - \sigma\sigma_{vvoo})}{NN_{kkt}},\ \text{if}_{BB} \le 22 \tag{3}$$

where s_u (kN/m^2) = shear strength of the crust layers estimated using CPT data from the ground surface to a depth of z_A as defined previously; K_o = coefficient of lateral pressure, which is assumed to be 0.5; ϕ_{cs} is the critical state friction angle which is assumed to be 33 degrees; and N_{kt} = 15 in the tip resistance (q_t) correlation used for clay. A sand-like soil with $I_B > 22$ will have a lower s_u than a crust layer composed of clay defined by $I_B < 22$, because the vertical effective stress is low at shallow depths. Thus, s_u represents the strength (and integrity) of the crust.

The liquefaction ejecta demand parameter captures the effects of system response mechanisms that the simplified liquefaction triggering procedure was never intended to capture. L_D also performs better than other liquefaction indices, such as liquefaction potential index (*LPI*, Iwasaki et al. 1978) and liquefaction severity number (*LSN*, van Ballegooy et al. 2014), because L_D applies the normalized-k_v as a weighting factor to the estimated h_{exc} at each depth in the soil profile. The performance of L_D is compared with the performance of *LSN* at thick clean sand sites and stratified silty soil sites in Christchurch in Figure 3.4 (Hutabarat and Bray 2022). Simplified liquefaction triggering procedures, *LPI*, and *LSN* overestimate the manifestation of liquefaction at stratified soil sites (e.g., *LSN* varies from 2 to 65 at sites that had no ejecta, Figure 3.4b). L_D resolves the overestimation tendency of the other liquefaction indices as its values are low (i.e., $L_D < 5$ except for two cases with $L_D = 10$) for 74 stratified silty soil sites that had no ejecta (Figure 3.4d). Additionally, L_D tends to be low at thick clean sand sites that had no ejecta, and L_D tends to be high for thick clean sites with severe and extreme ejecta severity. *LSN* also performs reasonably well at thick clean sand sites (Figure 3.4a); however, close examination of Figure 3.4a and 3.4c indicate L_D performs slightly better than *LSN* at these sites.

Combining the crust layer resistance parameter with the liquefaction ejecta demand parameter, both of which can be calculated using CPT data, improves the performance of the liquefaction-induced ejecta severity estimation because ejecta severity diminishes as the nonliquefiable crust layer becomes more resistant to ejecta formation. The resulting Hutabarat and Bray (2022) $L_D - C_R$ chart shown in Figure 3.5 estimates the severity of ejecta at level-ground, free-field sites. The $L_D - C_R$ chart generally estimates ejecta severity well for the 176 case histories investigated by Hutabarat and Bray (2022). Ejecta severity was categorized by the percentage of the total area within 20 m of the site covered by ejecta as described in Table 3.1. The true positive rate (*TPR*) calculated as $TPR = TP / (TP + FN)$, where TP = number of True Positive cases and FN = number of False Negative cases provides a quantitative measure of the efficacy of the $L_D - C_R$ chart and other liquefaction indices. *TPR* is 88% for the $L_D - C_R$ chart and 18% for *LSN* for the 74 cases that produced no ejecta in the Canterbury earthquakes (Hutabarat and Bray 2021). The chart resolves the overestimation problem of the other indices at highly stratified soil sites. The improvement is largely because L_D captures the important role of low-k_v layers by impeding upward seepage, which prevents ejecta production at stratified soil sites. *TPR* is 66%, 15%, 27%, and 74% for the $L_D - C_R$ chart and 49%, 46%, 20%, and 21% for *LSN* for thick clean sites with no ejecta (47 cases), minor ejecta (13 cases), moderate ejecta (15 cases), and severe ejecta (19 cases), respectively. Thus, in three of the four ejecta severity categories, the $L_D - C_R$ chart performs better than *LSN* at thick clean sites, and for two of these categories, the difference in the *TPR* values is significant.

3.3 Ejecta-Induced Ground Settlement

The field case history observations available to classify ejecta severity have generally been in the form of the percentage of an area of ground covered by ejecta. Ejecta coverage at a site is an indicator of ejecta-induced ground settlement. However, there are other factors to consider such as conditions that can produce a large volume of ejecta within a small area, such as due to a defect in the crust (i.e., light pole) or the presence of a reinforced concrete slab-on-grade foundation. Sites with localized ejecta produce more ejecta-induced settlement in these areas than sites with ejecta distributed over a broad area.

Tonkin+Taylor estimated localized and distributed ejecta-induced settlement and the percentage of area of ground covered by ejecta at many Christchurch sites using LiDAR surveys and field observations (van Ballegooy, personal communication, 2018). They related the localized and distributed ejecta-induced ground settlement measurements to the previously mentioned ejecta severity categories based on area covered by ejecta as shown in Table 3.1. The ejecta-induced settlement estimates based on the area covered by ejecta are rough. However, this approach enables an engineer to judge when localized structure settlement due to the ejecta mechanism will likely be 0 (None category), ≤ 50 mm (Minor category), ≤ 100 mm (Moderate category), or > 50 mm (Severe-Extreme categories).

The recent development of the Mijic et al. (2022) ejecta-induced settlement database provides an alternative approach. Mijic et al. (2022) developed 225 case histories that document the occurrence and quantity of ejecta for 61 free-field level ground sites affected by the 2010-2011 Canterbury earthquake sequence. Photographic evidence and aerial LiDAR measurements were used to estimate the amount of ejecta produced at the sites for the four primary Canterbury earthquakes. Areal ejecta-induced ground settlement was estimated over the entire selected assessment area, whereas localized ejecta-induced ground settlement was estimated over just the area covered by ejecta. This detailed examination of each case history provides a more robust estimate of ejecta-induced settlement than the rough estimates available previously. Each site was also characterized well by CPTs and other subsurface data.

The Hutabarat and Bray (2022) CPT-based $L_D - C_R$ chart was used to categorize the severity of the ejecta into the categories of None, Minor-Moderate, and Severe-Extreme. Categories were combined because the scatter in the localized ejecta-induced settlement case histories data did not justify the use of five distinct categories. The Mijic et al. (2022) free-field, level ground localized ejecta-induced ground settlement ranges of the three categories are shown in Table 3.2. The *TPR* is 79% for the Hutabarat and Bray (2022) estimate of 0 settlement for the 132 cases categorized as None in their $L_D - C_R$ chart, *TPR* is 85% for their estimate of ≤ 50 mm settlement for the 48 cases categorized as Minor-Moderate, and *TPR* is 71% for their estimate of 30 – 200 mm settlement for the 45 cases categorized as Severe-Extreme. Thus, the Hutabarat and Bray (2022) CPT-based ejecta severity chart designations of None, Minor-Moderate, and Severe-Extreme enables the engineer to estimate the free-field, level ground ejecta-induced settlement as either negligible, less than 50 mm, or 30 – 200 mm, respectively.

Table 3.2 should be used to estimate ejecta-induced ground settlement in most cases, because the relative quality of the data of the Mijic et al. (2022) study. The Tonkin & Taylor localized ejecta-settlement estimates of Table 3.1 are judged to be conservative. However, these values in Table 1 and the values in Table 3.2 should be considered when estimating localized structure settlement resulting from a defect in the crust or an adverse foundation condition because the values in Tables 3.1 and 3.2 bound the amount of potential localized ejecta-induced structure settlement.

Table 3.1. Ejecta severity and settlement from field surveys (van Ballegooy, personal communication 2018)

Ejecta Severity Category	Area within 20 m covered by ejecta (%)	Estimated localized ejecta-induced settlement (mm)	Estimated distributed ejecta-induced settlement (mm)
None	0	0	0
Minor	< 5	0 - 50	0 - 20
Moderate	5 - 20	0 - 100	10 - 50
Severe	20 - 50	50 - 300	25 - 150
Extreme	> 50	200 - 500	100 - 300

Table 3.2. Ejecta-induced settlement estimate using the Hutabarat and Bray (2022) ejecta severity chart

Ejecta Severity Category	Estimated free-field ejecta-induced ground settlement [a] (mm)
None	0
Minor- Moderate	≤ 50
Severe-Extreme	30 - 200

[a] Free-field, level ground localized ejecta-induced settlement estimated by Mijic et al. (2022)

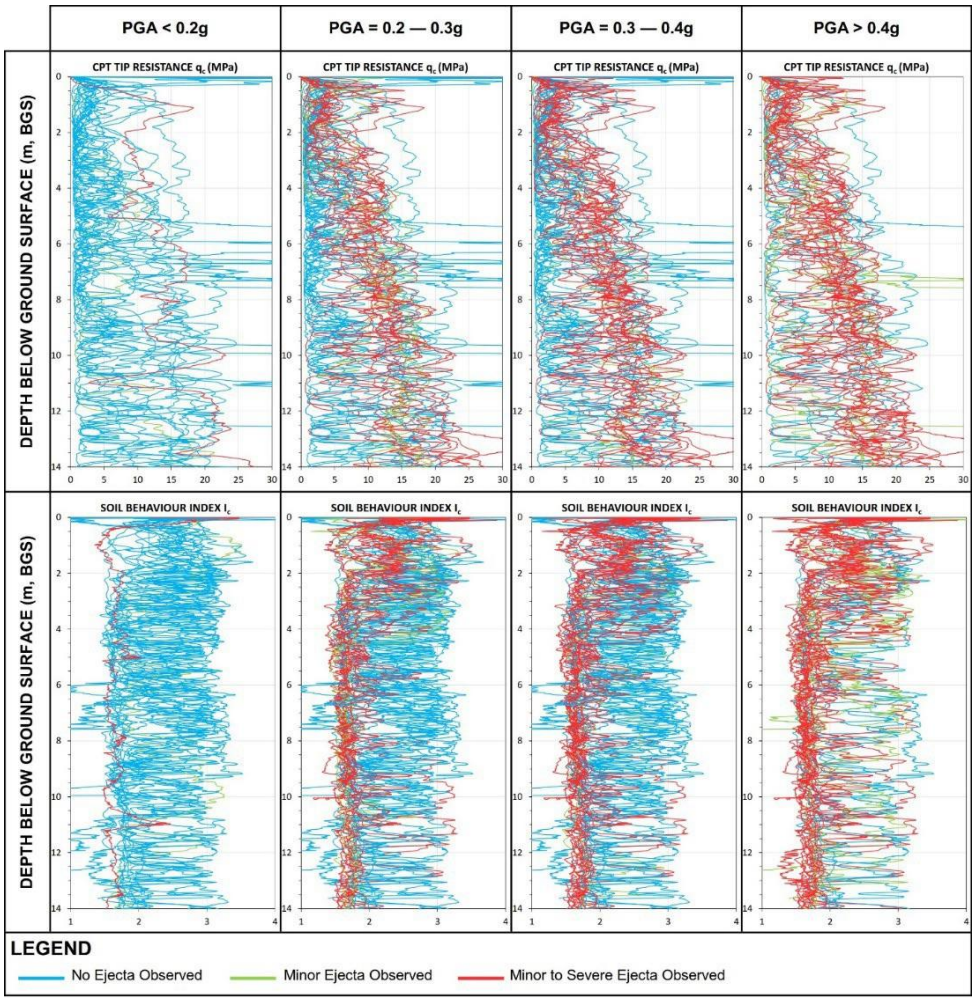

Figure 3.1. CPT tip resistance (q_c) and soil behavior type index (I_c) profiles for selected sites throughout Christchurch. Liquefaction observations are shown in: blue (no ejecta within 50 m radius of CPT), green (minor ejecta - < 5% of ground surface covered by ejecta within 50 m radius of CPT), and red (minor to severe ejecta – > 5% of ground surface covered by ejecta within 50 m radius of CPT) for the four main events of the Canterbury earthquake sequence for median PGA shaking levels for an equivalent M_w 6.0 event (from Beyzaei et al. 2018).

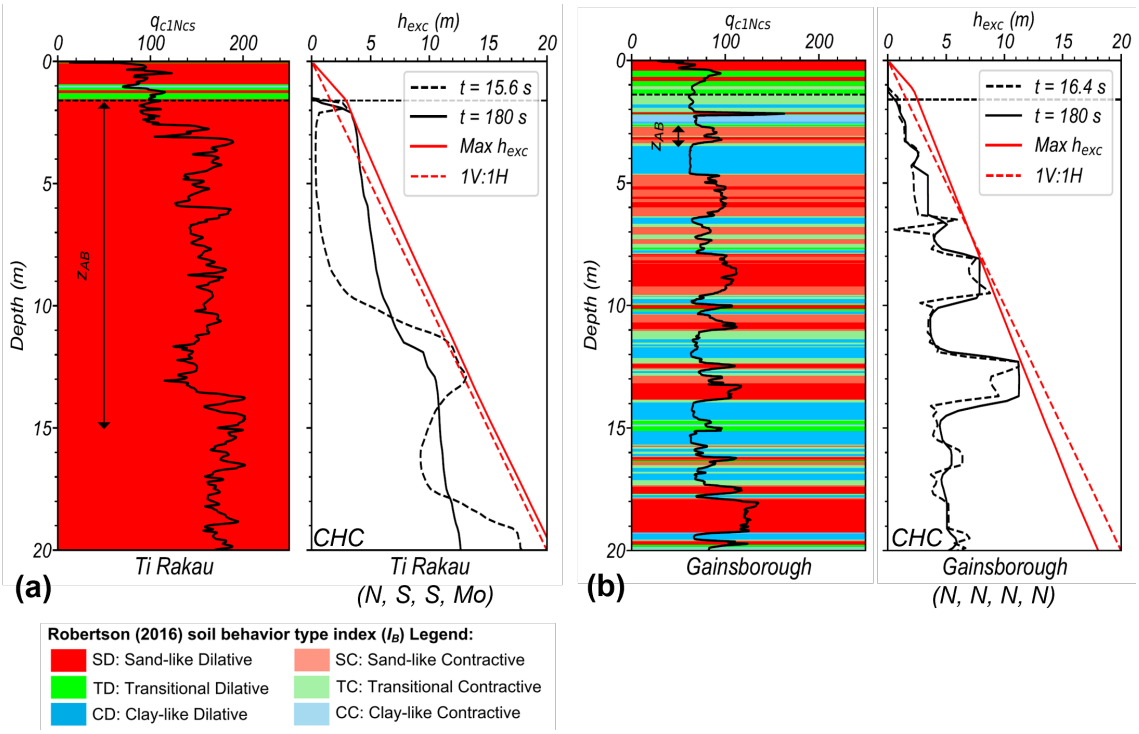

Figure 3.2. Representative thick sand (a) and stratified soil site (b) profiles of q_{c1Ncs}, modified soil behavior type index, and observed ejecta severity (given below site name in the sequence of the DAR, CHC, JUN, and DEC earthquakes where N = None; Mi = Minor; Mo = Moderate; S = Severe; E = Extreme).

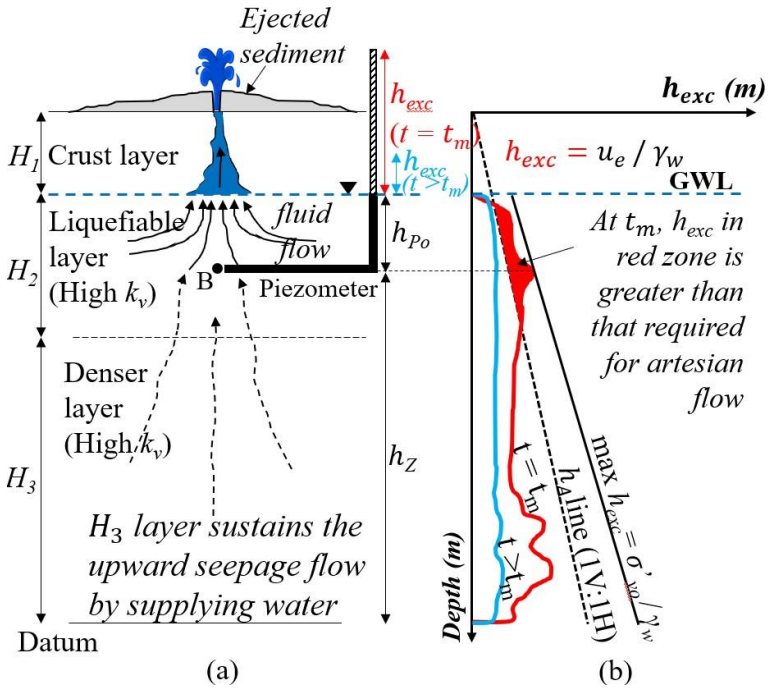

Figure 3.3. (a) Sediment ejecta mechanisms in a typical thick sand site and (b) Artesian Flow Potential concept.

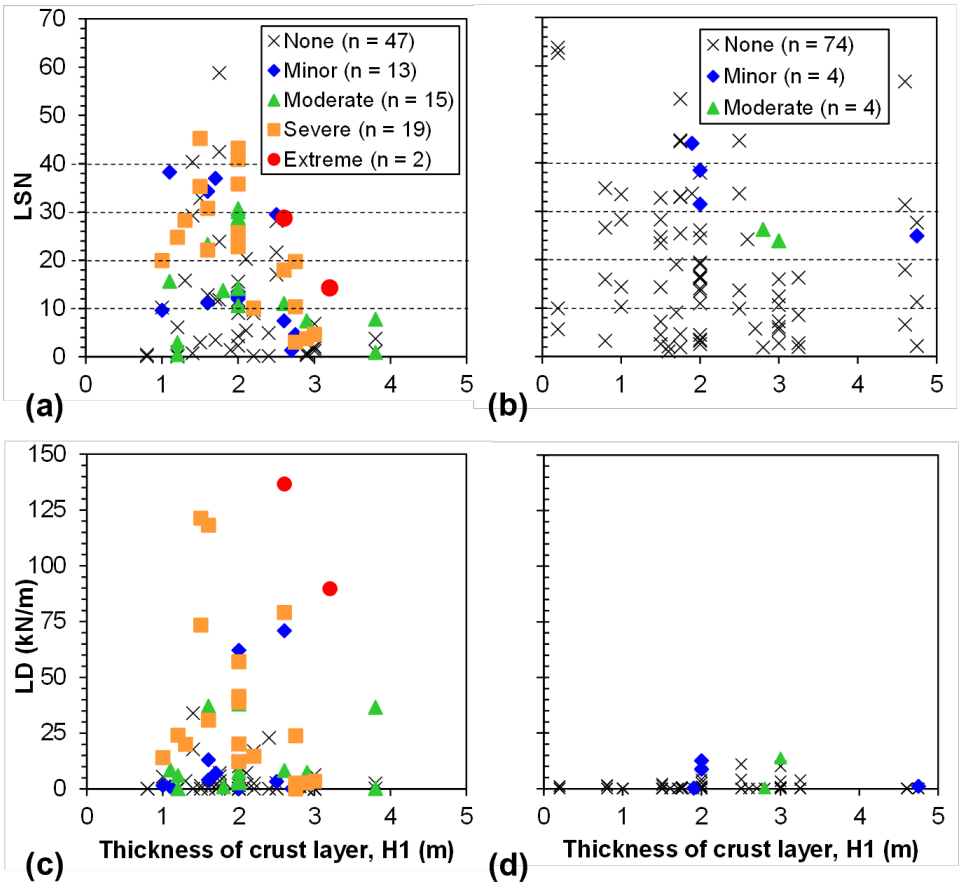

Figure 3.4. Distribution of liquefaction ejecta demand parameters vs. crust thickness for field case histories (from Hutabarat and Bray 2022)

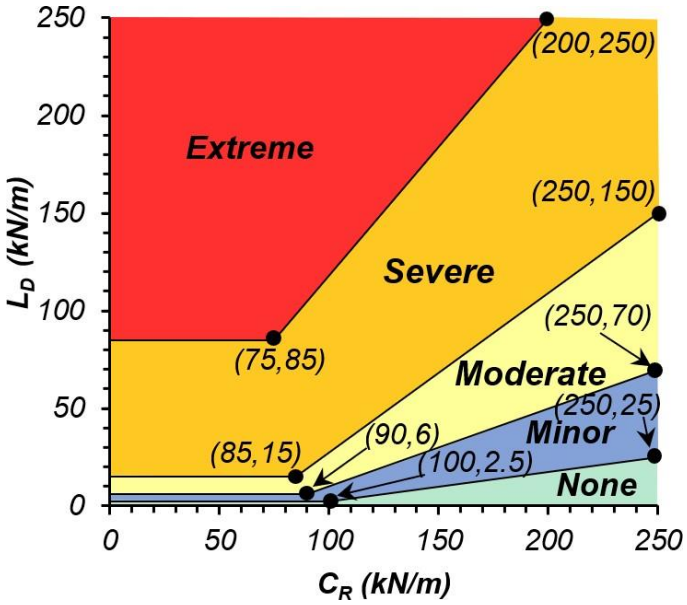

Figure 3.5. Liquefaction-induced ejecta severity chart defined by Liquefaction Demand (L_D) and Crust Resistance (C_R) parameters (Hutabarat and Bray 2022).

Chapter 4 SITE CHARACTERIZATION TO CAPTURE ELEMENT AND SYSTEM RESPONSES

4.1 Depositional Environment

The role of depositional environment should be considered in liquefaction assessments. Youd and Perkins (1978) recognized depositional environment as a key factor affecting liquefaction-induced ground failure. They emphasized the importance of considering sedimentation process, age of deposition, and geologic history. Seed (1979) highlighted the effects of soil fabric, overconsolidation ratio (OCR) and time under sustained loading. Laboratory testing by Ladd (1977) and Mulilis et al. (1977) showed different soil fabrics can change the *CRR* of sand test specimens with the same D_r by a factor of two. Seed (1979) recommended obtaining the "*best possible undisturbed samples*" and using considerable judgement to interpret how the characteristics of those samples will affect in situ liquefaction behavior of the deposit. Additionally, Seed (1979) noted even "*a single layer of relatively impervious fine sand or silt … would completely invalidate the results of pore pressure dissipation computations for vertical flow*." The findings from recent studies of system response (e.g., Cubrinovski et al. 2018a, Beyzaei et al. 2018a,b, and Hutabarat and Bray 2021a,b) also highlight the need to consider system response effects in conducting site investigations, laboratory tests, and analyses involving liquefaction.

4.2 Site Characterization Tools

Each project should start with a geologic assessment of the site and its surroundings. Much can be learned through the study of historical geologic maps and the evolution of the site (i.e., its depositional environment). For example, the 1850 geologic maps of Christchurch identified several streams that were buried as the city was developed, which liquefied in the 2011 Christchurch earthquake. Many of the zones of extensive liquefaction ejecta were located where old geologic maps depicted streams (e.g., Cubrinovski et al. 2011, Bray et al. 2014a, and Beyzaei et al. 2018b). Geophysical tests should follow with great insights possible through shear wave velocity (V_s) measurements. Subsurface explorations can follow to characterize the soil units that preliminary analyses indicate are likely to govern the seismic performance of the site.

The CPT is superior to the standard penetration test (SPT) in characterizing the state of sand, silty sand, nonplastic silt, and low-plasticity clayey silts that may be susceptible to liquefaction. The CPT has also been used successfully in sandy gravels with at least 30% sand (e.g., Bray et al. 2014b, Dhakal et al. 2022). The CPT provides a nearly continuous robust measurement of cone tip resistance (q_t), sleeve friction (f_s), and pore-water pressure (u_2), which are used to capture the response of soil to the penetration test. Measurement of V_s is also possible with the seismic CPT (SCPT) to capture the small strain stiffness of soil. The q_t and the derived parameters I_c and I_B characterize the state, compressibility, and strength of the soils penetrated by the CPT. I_c is superior to *FC* in characterizing soil compressibility (e.g., its effect on penetration resistance) so it is preferred. Estimating *FC* based on I_c is highly uncertain. Closely spaced high-quality sampling and CPTs by Beyzaei et al. (2020) confirmed conclusively there are large variations in *FC* in samples directly adjacent to zones with nearly constant I_c values in laterally consistent soil profiles. Additionally, numerous validated CPT correlations are available to estimate ψ_o, D_r, s_u, k_v, etc., in addition to *CRR*. Some disturbed soil samples should be retrieved for soil index testing to evaluate liquefaction susceptibility of intermediate soils (e.g., using the $PI \leq 12$ and $w/LL \geq 0.85$ criteria). It is insightful to perform field vane shear tests (FVST) to explore peak and remolded strength of clayey soils that are susceptible to strength loss.

High-quality "undisturbed" soil sampling of key soil units is prudent, especially for testing intermediate soils that are not well captured in the empirical database of the simplified liquefaction

triggering procedures. The Dames & Moore (DM) hydraulic fixed-piston thin-walled tube sampler can retrieve high quality samples of silt and silty sand (Markham et al. 2016), especially if the soil contains some clayey materials (Bray and Sancio 2006). As noted by Bray and Sancio (2008) and Boulanger and Idriss (2008), clayey silty soil can be sampled effectively. Cyclic testing can capture the cyclic response of these soils, which is invaluable to gaining insight on their likely performance and to calibrating soil constitutive models to support dynamic nonlinear effective stress analysis.

There is also value to performing high-quality continuous sampling to characterize geologic details and evidence of important features of depositional environment which are lost with conventional sampling. For instance, CPT, mini-CPT, and sonic borings did not adequately capture thin layering and soil fabric in Christchurch (Beyzaei et al. 2020). Conversely, detailed logging of high-quality samples captured the actual in situ layering at silty soil sites that did not manifest liquefaction though simplified liquefaction triggering procedures indicated they would at the Canterbury earthquake levels of shaking. Scanning electron microscope (SEM) images were useful to see the soil and potentially key characteristics not identified previously, such as soil fabric, cementation, and particle shape. Additionally, multiple groundwater measurement methods (e.g., piezometers, high-quality sampling, p-wave testing, and regional groundwater maps) were required to characterize complex groundwater conditions, including groundwater fluctuations.

4.3 Illustrative Example

Ground improvement was required to mitigate liquefaction effects to develop areas of Treasure Island, San Francisco, California. Simplified CPT-based liquefaction triggering methods indicated the entire surficial cohesionless soil deposit overlying the Young Bay Mud at the site would liquefy during the design events. ENGEO engineers, with external consultants that included professors from UC Berkeley, among others, performed a test program to evaluate the effectiveness of improving the liquefiable deposit with vibro-compaction by using the Direct Power Compaction (DPC) equipment (ENGEO 2016). Before ground improvement CPT tip resistances of the soil deposit are shown with the blue traces in Figure 4.1a in four cells of the ground improvement trials. The post-DPC CPT resistances are shown in red and green traces for CPTs performed 17 days and 31 days, respectively, after attempting to densify the surficial cohesionless soil deposit. The upper half of this unit was densified satisfactorily as evidenced by the significant increase in its q_c values. CPT tip resistances did not increase in the lower half of the unit. Application of the Robertson (2016) approach to differentiate soils with microstructure (e.g., cementation/bonding and aging) from "ideal soils" (e.g., young and uncemented) through the K^*_G parameter did not discern significant differences between the upper half and lower half of the unit as shown in Figure 4.1b.

DM sampling of the soil deposit was conducted to retrieve high-quality samples for CSS testing and to log in detail (ENGEO 2016). The upper half of the unit was clearly identified visually as a clean sand fill with few nonplastic fines. It was loose, young, and uncemented. Vibro-compaction effectively densified this material as expected. High-quality samples of the lower half of the unit revealed it was a highly reworked heterogeneous natural sandy shoal deposit with interlocking sand grains with clay bridges as shown in Figure 4.2. There was close grain packing with clay films bridging pores. At times the clay bridges were weakly developed with fewer fines, but the sand-size particles were packed into a stable arrangement of "interacting blocks" fabric as shown in the SEM images of Figure 4.2. The DPC equipment could not densify the natural shoal deposit because this deposit had a fabric that resisted densification through vibration. It was also more resistant to cyclic loading than the CPT-based simplified liquefaction triggering procedures indicated. High-quality continuous sampling provided engineers the information and insights required to consider these key issues in their evaluation of the seismic performance of the site.

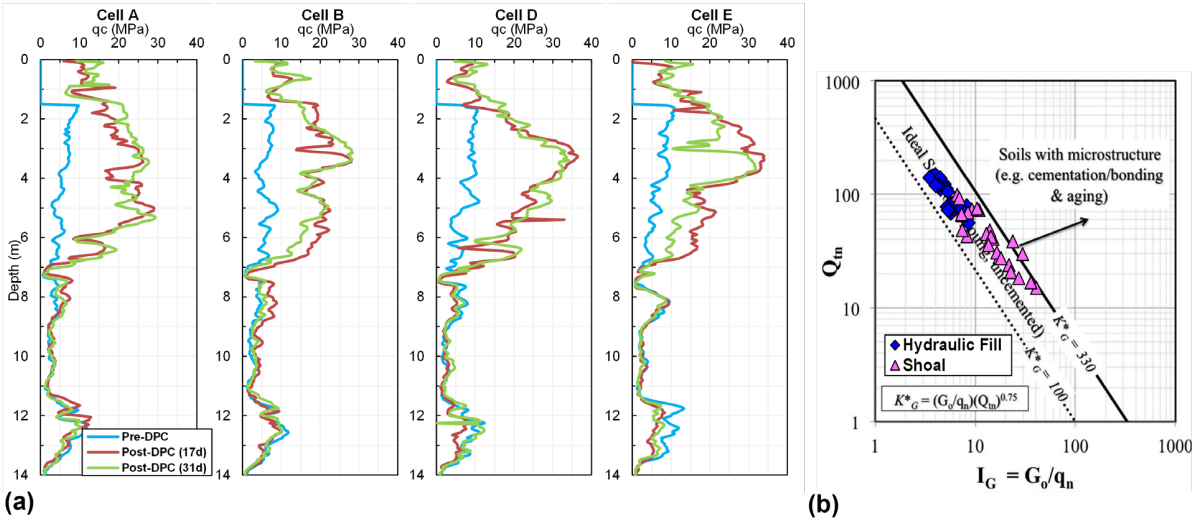

Figure 4.1. In situ characterization of the fill-shoal material at the ground improvement trial site at Treasure Island: (a) Pre-DPC and Post-DPC treatment CPTu profiles, and (b) data plotted on the Robertson (2016) Q_{tn}–I_G microstructure chart (data from ENGEO 2016).

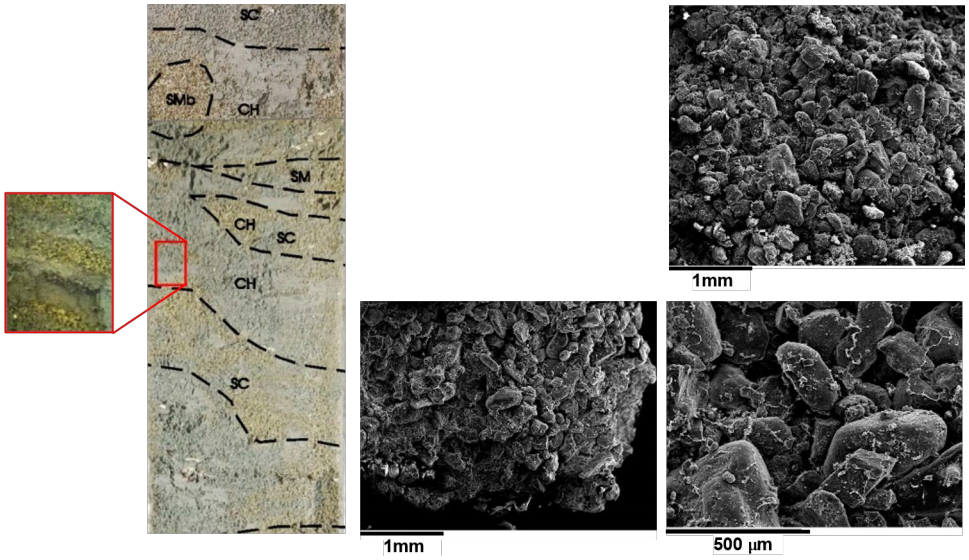

Figure 4.2. Detailed mapping of high-quality DM sample retrieved from Treasure Island shoal deposit (~11.1 m depth) with SEM images showing its fabric (~9.4 m) (ENGEO 2016).

Chapter 5 POST-LIQUEFACTION VOLUMETRIC-INDUCED GROUND SETTLEMENT

5.1 Motivation

Deterministic CPT-based post-liquefaction ground settlement procedures are widely used in practice (e.g., Zhang et al. 2002, and Idriss and Boulanger 2008). A probabilistic CPT-based post-liquefaction ground settlement procedure is required in support of performance-based earthquake engineering. Cetin et al. (2009) developed a probabilistic SPT-based post-liquefaction ground settlement procedure, but the CPT is superior to the SPT as discussed previously. Therefore, a probabilistic CPT-based post-liquefaction ground settlement procedure for free-field, level ground conditions is developed. It takes advantage of the results of a comprehensive database of laboratory tests with post-cyclic volumetric reconsolidation (Olaya and Bray 2022b) and a comprehensive database of field case histories of sites undergoing post-liquefaction volumetric-induced ground settlement (Olaya and Bray 2022a). In contrast, several of the current CPT-based post-liquefaction ground settlement procedures have comparisons against a limited number of case histories and they are based solely on the Ishihara and Yoshimine (1992) family of curves derived from CSS tests performed on one uniform clean sand (i.e., Fuji River Sand with FC = 0%, C_u = 3.2, D_{50} = 0.4 mm, e_{max} = 1.064, and e_{min} = 0.529) reconstituted to three different relative densities (i.e., 47%, 73%, and 93%) and tested at one vertical effective confining stress (i.e., 196 kPa). Although these methods have been shown to produce reasonable results, it has not been determined if the relationships developed from test data on just one uniform clean sand can be applied to other clean sands with other particle shapes and gradations, nonplastic silty sands, and nonplastic silts (Bray et al. 2017).

5.2 Post-Liquefaction Laboratory Tests

Olaya and Bray (2022b) developed a database of 579 test results on post-liquefaction volumetric strain (ε_v), including 299 test results that relate maximum shear strain (γ_{max}) to the factor of safety against liquefaction triggering (FS_L). The database includes post-cyclic test data on 10 clean sands, 2 gravels, 3 silty sands, 5 silts, and 3 clayey soils. The results of the numerous cyclic tests on a wide range of soil types enabled key trends of the effects of state, stress, soil type, gradation, etc. on the development of post-liquefaction volumetric strain to be identified. Their study found that uniform clean sand, gravel, nonplastic silty sand**,** and nonplastic silt test results could be captured in a unified manner using either D_r, ψ_o, or e_o to characterize the state of the soil. Post-liquefaction volumetric strain depended primarily on the state of the soil and the induced γ_{max}. The type of loading or effective confining stress (within the range of 40-400 kPa) were less important. Olaya and Bray (2022b) developed models using either D_r, ψ_o, or e_o as the independent variable to estimate ε_v for uniform clean sand, nonplastic silty sand, and nonplastic silt with quantification of the uncertainty of the estimate of volumetric strain. They also developed new models that estimate γ_{max} as a function of FS_L for uniform clean sand, nonplastic silty sand, and nonplastic silt with quantification of the uncertainty of the estimate. These experimentally based models can be used to inform the characteristics of an empirical CPT-based post-liquefaction model used to fit the case history data.

Like Ishihara and Yoshimine (1992) and several other researchers examining uniform sand data, D_r was examined first as the independent variable to characterize the state of the uniform nonplastic soil. Only nonplastic soils with coefficients of uniformity (C_u) < 4.5 were considered because D_r has been shown to be a reasonable parameter for comparing the state of different nonplastic soils if they are of uniform gradation. For instance, Bolton (1986) showed that the shear response of different clean sands can be grouped and characterized using D_r provided these sands are of similar uniform gradations.

Duncan et al. (2014) also showed D_r is an efficient parameter for characterizing the strength of granular materials of sands with similar C_u values. Whang (2001) analyzed seismically induced compression of different sands using D_r, and Duku et al. (2008) combined 16 different sands using D_r to develop a seismic recompression model appliable to a broad range of uniform sands. As discussed previously, Cubrinovski (2019) found D_r could be used to assess the liquefaction potential of nonplastic silty sand and tied directly to the D_r of uniform clean sand to compare responses of different soil types. Mijic et al. (2021a) also found comparable soil responses for uniform clean sand, uniform nonplastic silty sand, and uniform nonplastic silt with FC up to 70%.

5.3 Post-Liquefaction Volumetric Strain Models

Use of D_r enabled confirmation that uniform clean sands and uniform nonplastic silty sands at the same D_r under the same effective confining stress and sheared to the same γ_{max} develop similar ε_v as shown in Figure 5.1 (Olaya and Bray 2022b). The only data that are inconsistent with the overall trends are tests by Toriihara et al. (2000) of sand with compressible/crushable fine soil matrix with C_u = 18. All clean sand data shown in Figure 5.1a and silty sand data shown in Figure 5.1b have C_u < 4 and exhibit consistent responses. Similarly, uniform sand, uniform nonplastic silty sand, and uniform nonplastic silt test specimens at the same ψ_o develop similar ε_v when sheared to the same γ_{max} (Olaya and Bray 2022b).

Olaya and Bray (2022b) performed a series of nonlinear regression analyses of the uniform nonplastic soil data using different mathematical forms, first over the entire dataset and then over individual 10% bins of D_r (e.g., 50% to 60%) to find an efficient model. For a specific D_r bin of test results, ε_v increases directly proportionally to γ_{max} until it becomes constant at γ_{max} > 8%. The resulting model to estimate ε_v (in %) as function of γ_{max} (in %) for a specified value of D_r (in decimal) is:

$$\varepsilon_{vv} = 1.14 \cdot \exp(-2.0 \cdot D_r) \cdot \min(\gamma_{max}, 8\%) \cdot e^{\varepsilon} \quad (4)$$

where ε represents the model residuals which are normally distributed and unbiased with zero mean with σ = 0.62 in natural log units. Their bi-linear model and the ±1σ range for D_r = 70% - 80% are illustrated in Figure 5.2a where the observed data trends are captured well. The proposed model contours for D_r values from 30% to 90% are shown in Figure 5.2b along with the Ishihara and Yoshimine (1992) clean sand curves for comparison. The results of the regression analyses using the enlarged database indicate ε_v varies within a slightly narrower range than envisioned previously. It is important to capture these variations in ε_v in CPT procedures that track changes of D_r in a soil deposit.

Although the initial state parameter captures the volumetric strain potential of uniform clean sand, silty sand, and nonplastic silt in a unified manner, the ψ_o data are only one-fifth of the D_r data because the SSL is not determined in most testing programs (Olaya and Bray 2022b). Accordingly, their ψ_o model is preliminary. Additionally, there is greater uncertainty in estimating ψ_o in situ relative to estimating D_r. The model developed to estimate ε_v (in %) as function of γ_{max} (in %) for a specified value of ψ_o (in decimal) is:

$$\varepsilon_{vv} = 0.50 \cdot \exp(4.0 \cdot \psi_o) \cdot \min(\gamma_{max}, 8\%) \cdot e^{\varepsilon} \quad (5)$$

The model residuals are zero mean normally distributed with σ = 0.56 in natural log units. The proposed bi-linear model and the ±1σ range for ψ_o = -0.15 to -0.10 are illustrated in Figure 5.3a where the observed data trends are captured well. The proposed model contours for ψ_o values from -0.25 to 0.05 are shown in Figure 5.3b. Like the D_r-based models, the maximum ε_v varies within a range of about 1.5% to about 5% for the range of test data available. Overall, the ψ_o-based model performs reasonably well considering the limitations of the data (Olaya and Bray 2022b).

5.4 Post-Liquefaction Maximum Shear Strain Potential Models

Ishihara and Yoshimine (1992) recognized that initial liquefaction was triggered (FS_L = 1.0) in

numerous CSS tests at a single-amplitude shear strain ($\gamma_{cyc,SA}$) of about 3.5%, which is also consistent with the 5% double-amplitude axial strain ($\gamma_{cyc,DA}$) criterion often used with CTX tests. They also noted an inverse relationship between FS_L and γ_{max}. Initial regressions of the enlarged Olaya and Bray (2022b) database indicated that a hyperbolic relationship captures the FS_L - γ_{max} data trends well. To avoid having FS_L - ε_v curves at different D_r values cross when relating FS_L and strain potential, the model requires slightly different curvature once FS_L = 1.0 is crossed. Their hyperbolic model depends on one parameter (A) that is a function of D_r (in decimal) as

$$\gamma_{max} = 3.5 \cdot \left(\frac{2^{A} - FS_L^{A}}{2^{A} - 1} \right) \cdot \varepsilon_v^{\varepsilon} \qquad (6)$$

$$\gamma_{max} = 0; \quad \text{for } FS_L \geq 2.0$$

where

$$A = \begin{cases} -2.8 \cdot D_r^2 + 10.2 \cdot D_r - 9.8; & FS_L \geq 1.0 \\ -275 \cdot \exp(-6.6 \cdot D_r); & FS_L < 1.0 \end{cases}$$

The model residuals (ε) are zero mean normally distributed with $\sigma = 0.88$ in natural log units. The proposed FS_L - γ_{max} model for the D_r = 40-50% bin is shown in Figure 5.4 with the Yoshimine et al. (2006) model for comparison. The additional test data and the Ishihara and Yoshimine (1992) data show similar scatter with the Olaya and Bray (2022b) model deviating slightly from the Yoshimine et al. (2006) model. Differences in the models are larger for denser soils. There is not enough ψ_o data available to develop a robust FS_L - γ_{max} model for ψ_o. Olaya and Bray (2022b) developed a relationship to link ψ_o to D_r, so the D_r-based FS_L - γ_{max} could be used with the ψ_o-based γ_{max} - ε_v model to estimate post-liquefaction volumetric strain, which requires γ_{max} as an input.

5.5 Relating FS_L and Volumetric Strain Potential

Ishihara and Yoshimine (1992) developed a widely used chart to estimate ε_v or γ_{max} vs. FS_L as a function of a sand's D_r to estimate liquefaction-induced ground settlement or lateral spreading. The Olaya and Bray (2022b) models discussed previously provide alternative estimates of ε_v and γ_{max} using either D_r or ψ_o as a measure of the soil's state and FS_L as a proxy for the seismic demand. These models can be combined to estimate post-liquefaction volumetric-induced free-field ground settlement in a consistent manner. The models defined by Eqs. 4 and 6 describe the relationship between ε_v and FS_L as a function of D_r as shown in Figure 5.5. Importantly, the combined equations provide D_r curves that do not cross, unlike other models.

5.6 Post-Liquefaction Ground Settlement Field Case Histories

Post-liquefaction-induced ground settlement is a complex process resulting from the combined effects of particle sedimentation and soil reconsolidation due to post-shaking dissipation of excess pore-water pressure. Available CPT-based empirical models to estimate liquefaction-induced settlement for free-field level ground conditions are based on a limited number of field case histories. Consequently, it is difficult to quantify uncertainty in the estimate of post-liquefaction settlement with the limited number of field case histories available. To remedy this deficiency, Olaya and Bray (2022a) developed a database of 205 well documented ground settlement case histories to support the development of an improved probabilistic CPT-based liquefaction-induced ground settlement procedure. Their study takes advantage of the numerous site investigations, ground motion recordings, and LiDAR surveys performed following the 2010-2011 Canterbury earthquake sequence and the 2013-2016 northern South Island, New Zealand earthquakes.

Obtaining field case histories with reliable pre- and post-earthquake ground surface elevation measurements is the primary limitation in the development of post-liquefaction ground settlement case histories. CPT-based investigations and topographic surveys conducted by the US Geological Survey

(USGS) following the 1989 Loma Prieta earthquake produced some of the first CPT-based well-documented case histories of post-liquefaction settlement. Additional case histories have gradually become available. However, the reconnaissance efforts conducted in Christchurch after the 2010-2011 Canterbury earthquakes produced an unparalleled amount of diverse and high-quality data with ground motion recordings, ground performance observations for four major earthquakes, aerial imagery, LiDAR measurements, and subsurface characterization, largely through CPTs. Research teams developed an initial set of 55 well documented sites to investigate cases where none-to-minor land damage was observed even though simplified liquefaction methods estimated severe surface manifestations (e.g., Russell and van Ballegoy 2015, and Cubrinovski et al. 2018a). Mijic et al. (2022) developed 34 additional sites with the objective to include sites with and without liquefaction manifestations that show no major discrepancies between the estimates from simplified liquefaction methods and the actual field observations. Free-field, level ground sites in these two datasets were examined to enlarge the post-liquefaction ground settlement database. Additionally, well documented sites in Wellington, New Zealand that experienced three major earthquakes, including the 2016 Kaikoura earthquake, were added to the Olaya and Bray (2022a) database. The final compilation of free-field level ground post-liquefaction settlement case histories by Olaya and Bray (2022a) is summarized in Table 5.1. There are 205 case histories at sites described by 967 CPTs with reliable ground settlement measurements.

Olaya and Bray (2022a) defined a case history as the combination of: (1) a site with laterally uniform soil stratigraphy with at least one CPT, (2) an earthquake event represented by its M_w, ground surface *PGA* or other intensity measures, and (3) consistent post-liquefaction volumetric-induced free-field, level ground settlement measurements. A site is not defined by a CPT. Instead, a site is defined by its consistent geology and seismic performance. Thus, each case history is a site characterized by a geometric mean set of CPT-derived parameters, which undergoes an estimated level of earthquake shaking, wherein the liquefaction-induced ground settlement was measured. Sites characterized by several CPTs are valuable as they capture the average subsurface conditions and the variability of the CPT parameters across a site. For sites with multiple CPT soundings or multiple point settlement measurements, geometric means of these values are used to represent central values in the case history.

An illustrative definition of a case history is depicted in Figure 5.6. The stratigraphy, soil types, and the effects of liquefaction experienced at CentrePort in Wellington after the 2013 Cook Strait, 2013 Lake Grassmere, and 2016 Kaikoura earthquakes have been documented extensively (e.g., Cubrinovski et al. 2018b, Dhakal et al. 2020, and Dhakal et al. 2022). CPT data were collected through a collaborative research effort led by the Univ. of Canterbury with the Univ. of California, Berkeley, Tonkin + Taylor, Ltd., and CentrePort. Site 4 is within a part of CentrePort built with dumped sandy gravel fill. The sand-silt fractions of the gravelly fill are between 30% and 70%. The CPT data (e.g., q_{c1n}, I_c,) and liquefaction parameters (e.g., FS_L, and *LSN*) were used to define the extent of a site. They are relatively consistent for the 6 CPTs advanced in Site 4. Additionally, the surveyed ground settlement varies within 200 mm to 350 mm across most of the site. Lastly, the M_w of the earthquake events are known, and *PGA* can be estimated with confidence with nearby strong motion stations that are not affected by liquefaction.

Reclaimed land is typically the product of sequential hydraulic filling of borrowed granular material. This construction method results in relatively uniform and loose fills typically overlying marine sediments. The hydraulic fills in the database are usually less than 10 m thick and are typically comprised of silty sands to sandy silts (with exception of CentrePort which has a significant fraction of gravel). Case histories of the performance of hydraulic fills, such as those during the 1995 Kobe earthquake (e.g., Yasuda et al. 1996), indicate that uniformly constructed hydraulic fills tend to exhibit relatively uniform settlement. Conversely, natural soil deposits are inherently heterogenous because of complex depositional processes that can show significant spatial variability in addition to other age-related effects. The assessment of liquefaction performance in the Christchurch illustrates the effects of depositional processes on ground performance (Beyzaei et al. 2018a). Due to their differing formation processes and seismic performance, the case histories are classified into the two primary categories of natural soil deposits and hydraulic fills. Of the 205 case histories, 163 cases are natural soil deposits and 42 cases are hydraulic fills.

Table 5.1 Summary of Free-Field Settlement Case Histories

Location	Earthquake	Case histories	CPTs	Type of deposit
Marina District, California	1989 Loma Prieta	4	8	Hydraulic fill
Treasure Island, California		5	84	
Wufeng, Taiwan	1999 Chi-Chi	3	3	Natural soil
Yuanlin, Taiwan		3	4	
CentrePort, Wellington	2013 Cook Strait	1	8	Hydraulic fill
	2013 Lake Grassmere	13	69	
	2016 Kaikoura	13	69	
Christchurch, New Zealand	2010 Darfield	45	210	Natural soil
	2011 Christchurch	47	220	
	2011 June	65	285	
Urayasu, Japan	2011 Tohoku	6	6	Hydraulic fill

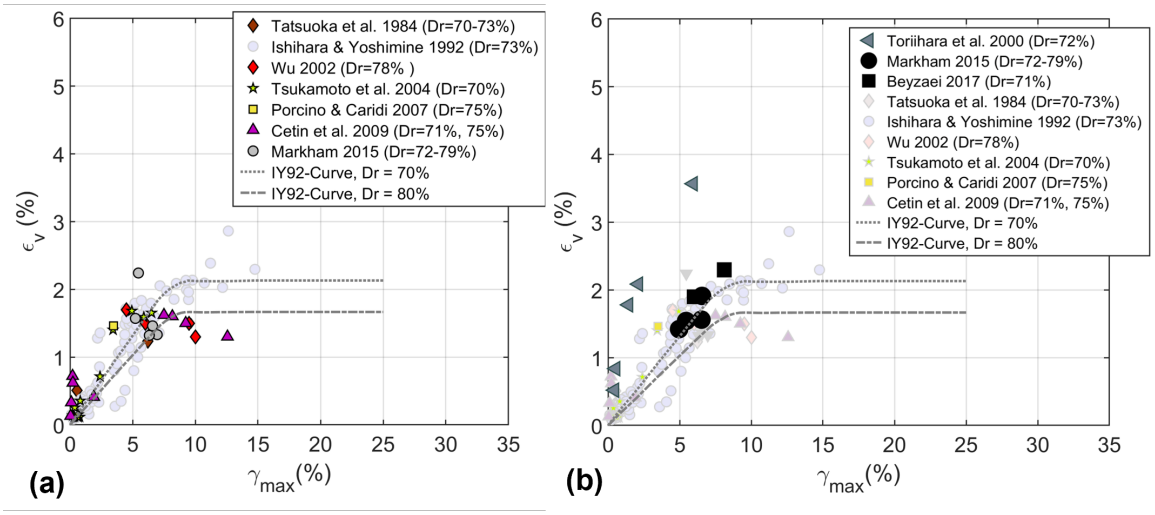

Figure 5.1. Volumetric strain vs. maximum shear stress test data for D_r = 70% - 80: (a) Clean uniform sand (Ishihara and Yoshimine 1992 clean sand data are shown in light blue), and (b) nonplastic to low-plasticity silty sand (clean uniform sand data shown in light blue) (Olaya and Bray 2022b).

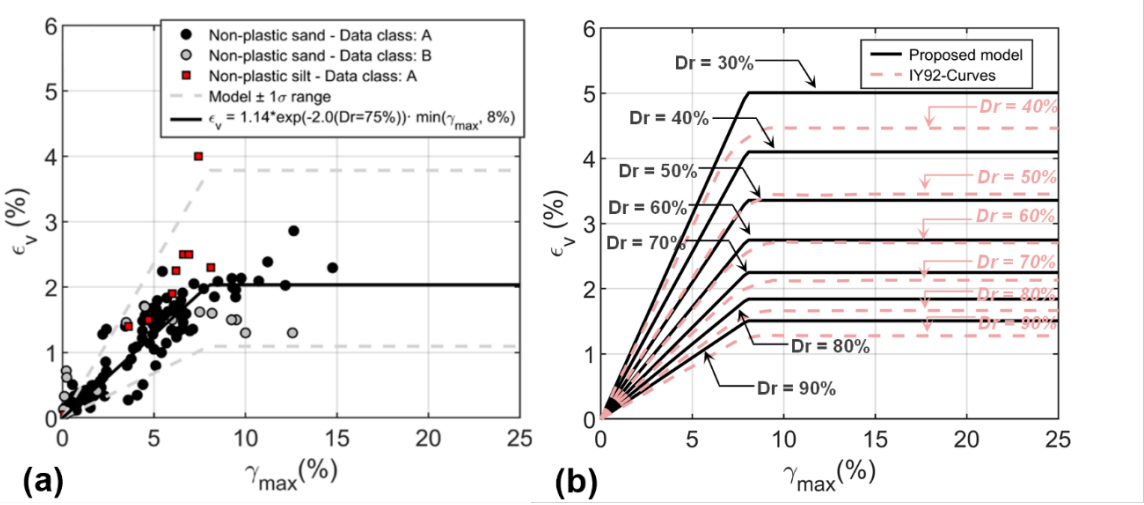

Figure 5.2. Nonplastic uniform soil $\varepsilon_v - \gamma_{max}$ proposed model in terms relative density: (a) D_r = 70% - 80%, and (b) model contours (Olaya and Bray 2022b).

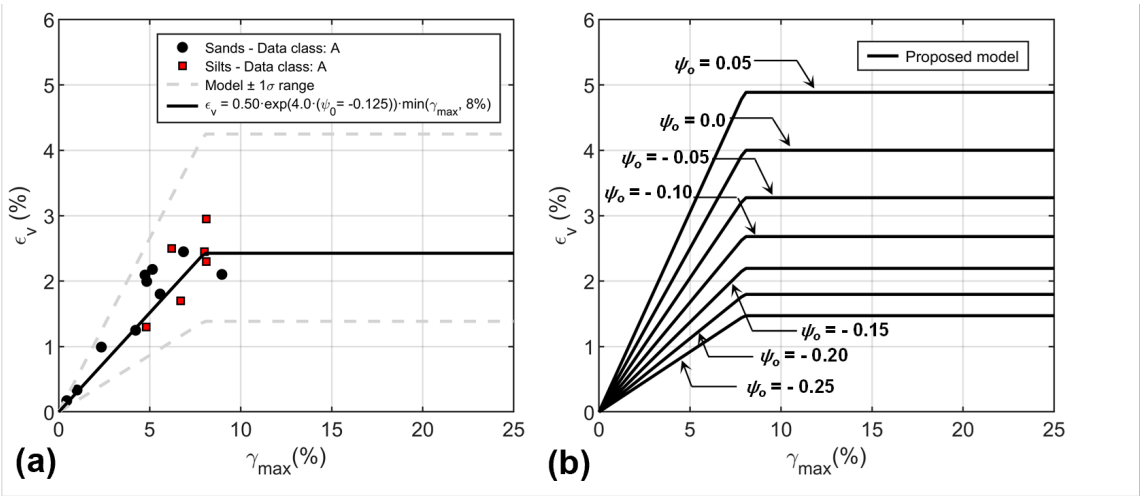

Figure 5.3. Nonplastic uniform soil $\varepsilon_v - \gamma_{max}$ proposed model in terms of state parameter: (a) ψ_o = -0.15 to -0.10, and (b) model contours (Olaya and Bray 2022b).

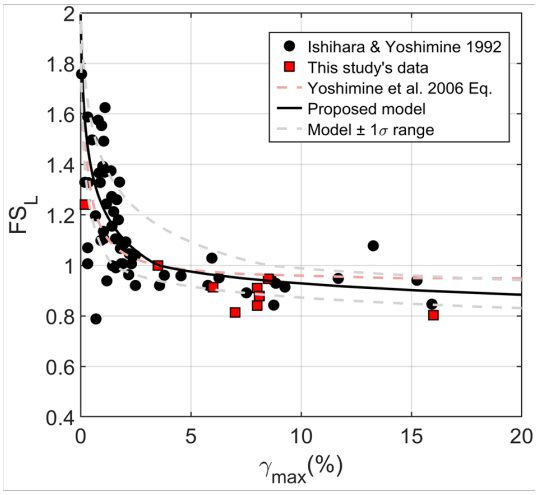

Figure 5.4. γ_{max} – FS_L data and proposed model in terms relative density for D_r = 40% - 50% (Olaya and Bray 2022b).

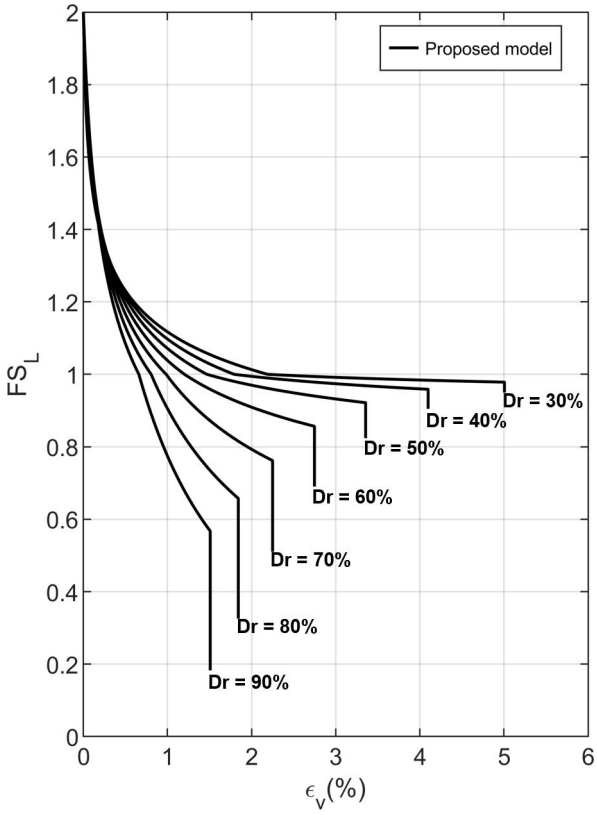

Figure 5.5. Relationship between ε_v and FS_L in terms of D_r (Olaya and Bray 2022b)

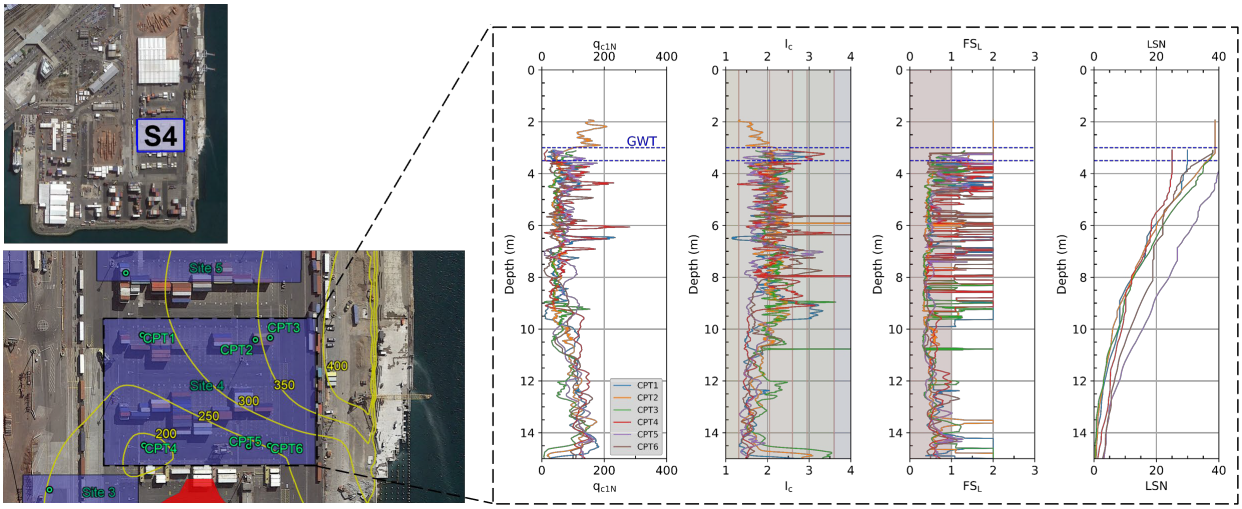

Figure 5.6. CentrePort with enlarged image of Site 4 showing CPT locations and mean ground settlement (mm) contours with q_{c1n}, I_c, FS_L, and LSN profiles (data from Dhakal et al. 2022, Olaya and Bray 2022a). Images from Google Earth®

Chapter 6 PROBABILISTIC CPT-BASED LIQUEFACTION GROUND SETTLEMENT PROCEDURE

6.1 Framework of the Procedure

The proposed probabilistic CPT-based liquefaction ground settlement procedure employs the framework of Ishihara and Yoshimine (1992), which is the framework used in many procedures (e.g., Zhang et al. 2002, and Idriss and Boulanger 2008). The post-liquefaction volumetric ground settlement (S_v) is calculated initially as

$$FF_{vv} = \sum_{ii} \varepsilon\varepsilon_{vv_{ii}} \cdot \Delta ZZ_{ii} \tag{7}$$

where $\varepsilon\varepsilon_{vv_{ii}}$ is the post-liquefaction volumetric strain calculated using the Olaya and Bray (2022b) model for all nonplastic soils, which is calculated using either its D_r-based or ψ_o-based FS_L-γ_{max} and γ_{max}-ε_v relationships in which FS_L and D_r or ψ_o are estimated using CPT data at each depth i, and ΔZ_i is the thickness of the unit at depth i.

The probabilistic procedure was developed using the mean FS_L at a probability of liquefaction triggering (P_L) of 50% calculated using two simplified liquefaction triggering procedures: (1) the Robertson and Wride (1998) procedure as updated by Robertson (2009) and converted to a probabilistic method by Ku et al. (2012), and (2) the Boulanger and Idriss (2016) procedure. The intent is to use an unbiased estimate of FS_L that captures part of the epistemic uncertainty in estimating FS_L. Use of P_L = 15% produces a conservative estimate of FS_L and hence a conservative estimate of S_v. Use of one simplified liquefaction procedure or alternative procedures changes the estimate of FS_L in a manner dependent on the procedure(s) employed.

The proposed probabilistic post-liquefaction ground settlement procedure also requires a CPT-based estimate of D_r or ψ_o. CPT-based correlations to estimate D_r are based on clean sand data (e.g., Tatsuoka et al. 1990). Correlations to estimate D_r as a function of CPT data in silty soil do not exist. To address this shortcoming, D_r data of high-quality DM nonplastic soil samples retrieved by Markham (2015) and Beyzaei (2017) within 2 m of CPTs in Christchurch were compiled and examined. These data are shown in Fig. 6.1 in terms of q_{c1n}/D_r^2 vs. I_c. The q_{c1n}/D_r^2 relationship is widely used for clean sand (Robertson and Cabal 2015). The data in Fig. 6.1 enables it to be used for silty soils as a function of soil compressibility represented by I_c. The ratio q_{c1n}/D_r^2 decreases as soil compressibility increases (i.e., as I_c increases), because the CPT tip resistance decreases in more compressible soils if the soils have the same D_r. The proposed relationship was extended to capture sand with I_c < 1.6 using an average of the existing CPT-based D_r correlations for clean sand with q_{c1n}/D_r^2 = 290 as shown in Eq. 8 where D_r is expressed in decimal. The model residuals (ε) are zero mean normally distributed with σ = 0.31 in natural log units.

$$DD_{rr} = \begin{cases} \sqrt{\dfrac{qq_{cc1nn}}{290}} & \text{for } II_{cc} < 1.6 \\ \sqrt{\dfrac{qq_{cc1nn}}{1500}} & \text{for } 1.6 \le II_{cc} \le 2.6 \end{cases} \tag{8}$$

As an alternative to the proposed model, the Robertson and Cabal (2015) CPT-based D_r correlation for clean sand is used. It is extended to capture silty soils with I_c > 1.64 using the clean sand correction factor (K_c) of Robertson and Wride (1998) with a compressibility factor of 350. The resulting relationship is also shown in Figure 6.1. The average of the two D_r values estimated by these CPT

correlations is used in the development of the post-liquefaction ground settlement procedure to capture partially the epistemic uncertainty of the estimate of D_r.

The average of two CPT-based correlations to estimate ψ_o is also used for the ψ_o-based volumetric strain model. Robertson (2010) developed a correlation to estimate ψ_o based on clean sand equivalent resistance ($Q_{tn,cs}$). As an alternative to this correlation, Olaya and Bray (2022b) developed a CPT correlation to estimate ψ_o based on clean sand and nonplastic silty sand and silt laboratory data with a generic SSL equation based on Bolton (1986) dilatancy index resulting in estimating ψ_o as

$$\psi_o = e_o - e_{ccc} = \xi \cdot (e_{max} - e_{min})\,[1/\ln(\sigma'_{cr}/\sigma'_c) - D_r] \tag{9}$$

where σ'_{cr} is soil's crushing stress, σ'_c the effective normal/confining stress, and ξ is introduced as an adjustment factor that accounts for the assumptions required to convert the Bolton (1986) equation into Eq. 9 and the variability of the individual relationships used to develop Eq. 9 (e.g., variability in estimation of $e_{max} - e_{min}$). The ξ factor was developed through a calibration process using data from 60 laboratory tests to account for the sources of error in the approximation of Eq. 9 as

$$\xi = 0.724 \cdot \exp(-0.031 \cdot FFCC) \tag{10}$$

where FC is expressed in percent as an integer. Examination of Eq. 9 showed the estimate of ψ_o is not too sensitive to σ'_{cr}, so typical values provided by Mitchell and Soga (2005) are used (i.e., 8000 kPa for silt; 10000 kPa for silty sand; and 20000 kPa for clean sand). The average of the soil-dependent correlation of Cubrinovski and Ishihara (2002) is used to estimate $e_{max} - e_{min}$ with typical values of 0.45 for clean sand, 0.65 for silty sand, and 0.80 for silt.

6.2 Adjustments and Calibration of the Model

The residuals obtained using Eq. 7 with two methods to estimate liquefaction triggering and two methods to estimate relative density or the state parameter showed differences between its estimates for natural soil deposits and hydraulic fills as expected due to their different depositional processes. Residuals are calculated as $\ln(S_{v\_meas}) - \ln(S_{v\_est})$, where S_{v_meas} is the mean measured settlement and S_{v_est} is estimated from Eq. 7 using the Olaya and Bray (2022b) post-liquefaction volumetric strain model presented previously. The natural soil deposits residuals show a constant overall offset. In addition, evaluation of the distribution of residuals shows bias as a function of a site's average I_c. Further evaluation of the hydraulic fill residuals with M_w as high 9.1 shows bias as a function of M_w. Based on these observations, a calibration factor (C), a soil behavior factor (SB), and a magnitude factor (MF) are incorporated in the final model. The calibration and correction factors are developed using the residuals yielded by the D_r-based model, and these factors are then applied to the ψ_o -based model because there is greater confidence at this time in the D_r -based model because it has more data and more established correlations to estimate D_r. Several depth-weighting factors (e.g., Cetin et al. 2009, van Ballegoy et al. 2014) were investigated but a depth-weighting factor was not incorporated in the model because it did not reduce the standard deviation or the bias in the model. Moreover, sensitivity studies found the use of a depth-weighting factor made mechanistically incorrect adjustments to the post-liquefaction ground settlement estimate as a liquefiable layer of variable thickness was moved up and down in simplified soil profiles.

First, the offset present in clean sand natural soil sites is estimated from the distribution of residuals for sites with average $I_c < 1.8$. This offset results in a calibration factor of $C = 1.5$. This factor is due to inherent differences between the characteristics of natural soil deposits and the largely reconstituted or slightly disturbed soils used in the laboratory tests that form the basis of the Olaya and Bray (2022b) post-liquefaction volumetric strain model (e.g., soil fabric, time under sustained loading, OCR). The calibration factor is largely controlled by the Christchurch case histories because most of the natural soil deposit data are from Christchurch. It was adjusted slightly in consideration of the different

bias of the non-Christchurch data. The calibration factor is not required for hydraulic fills because the characteristics of hydraulic fills are better captured by the soils tested in the laboratory (i.e., C =1.0 for hydraulic fill).

After C is applied to the results, residuals are plotted against I_{c15} and the biases shown in Figures 6.2a and 6.2b for hydraulic fills and natural soil deposits, respectively, are eliminated by applying a soil behavior factor (SB) shown in Figure 6.2c and calculated as

$$FFSS = \exp\left(-0.415 \cdot \max\left(II_{cc_{15}}, 1.8\right) + 0.747\right) \quad (11)$$

where I_{c15} is the average I_c over a depth of 15 m. A depth of 15 m was selected from exploratory statistical analyses of the depth that contributes significantly to settlement. There are not strong differences between the biases of the natural soil deposit data and hydraulic fills data, so the same SB value is applied to all data for consistency. Additionally, the same SB value can be applied to the D_r-based and the ψ_o-based models without introducing significant biases.

Most of the bias in the residuals of the proposed model are eliminated after application of C and SB; however, a bias remained as a function of earthquake moment magnitude. Duration is captured in the calculation of FS_L through the magnitude scaling factor (MSF). Initially another magnitude scaling factor was not thought to be required. However, the residuals indicated a dependence on M_w as shown in Figures 6.3a and 6.3b for hydraulic fills and natural soil deposits, respectively. The biases in these residuals are eliminated by applying a Magnitude Factor (MF) as

$$MMFF = \exp(0.225 \cdot MM_{ww} - 1.575) \quad (12)$$

The variation of MF with M_w is shown in Figure 6.3c with the Idriss and Boulanger (2008) MSF for comparison. In retrospect, laboratory testing on sand specimens by Lee and Albaisa (1974) found that additional loading cycles applied beyond initial liquefaction induced larger volumetric strains, which indicates that larger M_w earthquakes with a larger number of equivalent cycles of loading should induce larger settlement. The same MF value is applied to natural soil deposits and hydraulic fills using either the D_r-based or the ψ_o-based volumetric strain models.

6.3 Final Model

The proposed probabilistic model to estimate free-field post-liquefaction ground settlement is

$$FF_{vv} = CC \cdot MMFF \cdot FFSS \cdot \sum_{ii}\left[\varepsilon\varepsilon_{vvii} \cdot \Delta dd_{ii}\right] \cdot ee^{\varepsilon\varepsilon} \quad (13)$$

where the error term ε is normally distributed with zero mean and σ = 0.53 in natural log units for hydraulic fill and σ = 0.63 in ln units for natural soil for the D_r-based volumetric strain model, and σ = 0.52 in ln units for hydraulic fill and σ = 0.63 in ln units for natural soil for the ψ_o-based volumetric strain model. As expected, the uncertainty is lower estimating post-liquefaction ground settlement in constructed hydraulic fills than in natural soil deposits. Also, C = 1.0 for hydraulic fills and C = 1.5 for natural soil deposits for the reasons mentioned previously. Eq. 11 is used to calculate SB as a function of I_{c15}, and Eq. 12 is used to calculate MF as a function of M_w. As described previously, $\varepsilon\varepsilon_{vv_{ii}}$ is the post-liquefaction volumetric strain calculated using the Olaya and Bray (2022b) model, which is calculated using either its D_r-based or ψ_o-based FS_L-γ_{max} and γ_{max} - ε_v relationships in which FS_L and D_r or ψ_o are estimated using CPT data at each depth i, and ΔZ_i is the thickness of the unit at depth i. The model is based on the mean estimate of FS_L with P_L = 50% using the two simplified liquefaction triggering produces mentioned previously and on the mean estimate of D_r or ψ_o using the two procedures mentioned previously.

The residuals for the proposed probabilistic model for hydraulic fills and natural soil deposits are shown in Figures 6.4a and 6.4b, respectively. The proposed model provides reasonable estimates of

ground settlement. The error term in the probabilistic model describes the uncertainty in the estimate of S_v given the values of the input parameters. In a deterministic assessment, the post-liquefaction ground settlement should be provided as a likely range of settlement using the 16% and 84% values from Eq. 13 [i.e., (median S_v) $\cdot e^{-\sigma}$ and (median S_v) $\cdot e^{+\sigma}$ values]. In a probabilistic assessment, the additional uncertainty of the input parameters required to calculate S_v using Eq. 13 and the underlying models described in this report can be considered by including the uncertainty in the estimate of the ground motion parameter *PGA* in a seismic hazard assessment and by capturing the uncertainty in the key input parameters and models through a logic tree approach.

6.4 Illustrative Application of the Procedure

The application of the proposed liquefaction-induced volumetric-induced ground settlement procedure is illustrated using two case histories described in Olaya and Bray (2022a).

Case history CP-K16-S4 is a hydraulic fill site located in Wellington, New Zealand. The ground settlement is estimated for the 2016 Kaikoura M_w 7.8 earthquake that generated a nonliquefied site ground surface PGA = 0.25 *g*. The site has 10 to 20 m thick silty/sandy gravel fill atop marine sediments and alluvium that do not liquefy. The site is characterized by the 6 CPTs shown in Fig. 5.6 with the groundwater table located between 3.0 m to 3.5 m below the ground surface. I_{c15} varies between 1.91 to 2.25 for the 6 CPTs. The average of the D_r estimated using Eq. 8 and Robertson and Cabal (2015) varies between 30% and 95% in the profile and the average of the P_L = 50% FS_L estimated using the Boulanger and Idriss (2016) and Robertson and Wride (1998)/Robertson (2009)/Ku et al. (2012) procedures varies between 0.30 and 2.0. Use of Eqs. (4) and (6) with the average D_r and FS_L values at each depth in the profile provides estimates of ε_v between 0 and 4.0%. *SB* is estimated to be between 0.83 and 0.96 using Eq. (11). *MF* is estimated as 1.19 using Eq. (12). C = 1.0 because it is a hydraulic fill. The median estimate of settlement for each of the 6 CPTs using Eq. (13) is between 250 mm and 410 mm with the site's geomean value of S_v = 330 mm and the 16% to 84% range of 190 mm to 560 mm (σ = 0.53). The estimated range of ground settlement is consistent with the surveyed ground settlement range of 200 mm – 350 mm (Dhakal et al. 2020).

Case history Ch-S167 is a natural soil deposit site located in Christchurch, New Zealand. Ground settlement is estimated for the 2011 M_w 6.2 June earthquake with a nonliquefied site ground surface PGA = 0.29 *g*. The site profile is composed primarily of silty sand layers with occasional lenses of clayey soil. The groundwater depth is estimated to be 2.0 m, and 3 CPTs are available at this site (Olaya and Bray 2022a). I_{c15} varies between 1.63 to 1.79. Following the same procedure as in the previous example, the average D_r varies between 20% and 90% in the profile and the average of the P_L = 50% FS_L varies between 0.60 to 2.0. Use of Eqs. (4) and (6) with the average D_r and FS_L values at each depth provides estimates of ε_v between 0 to 3.6%. *SB* is estimated to be 1.0 (I_{c15} < 1.8), *MF* = 0.84, and C = 1.5 (natural soil deposit). The median estimate of settlement for each of the 3 CPTs using Eq. (13) is between 50 mm and 80 mm with the site's geomean value of S_v = 60 mm and the 16% to 84% range of 30 mm to 110 mm (σ = 0.63). The estimated range of ground settlement is consistent with the LiDAR-based measured settlement range of 30 mm – 90 mm (Olaya and Bray 2022a).

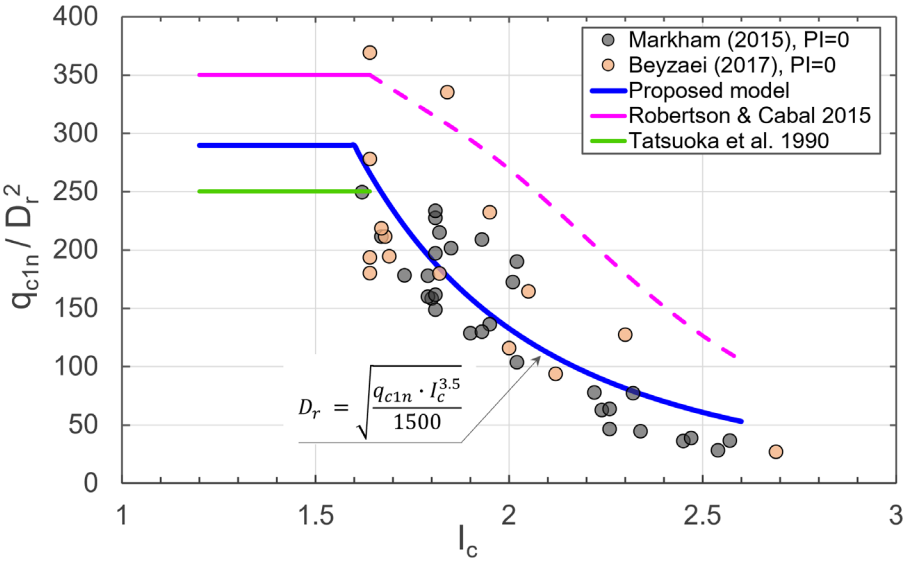

Figure 6.1. Influence of soil compressibility (through I_c) on the ratio of CPT tip resistance to D_r^2

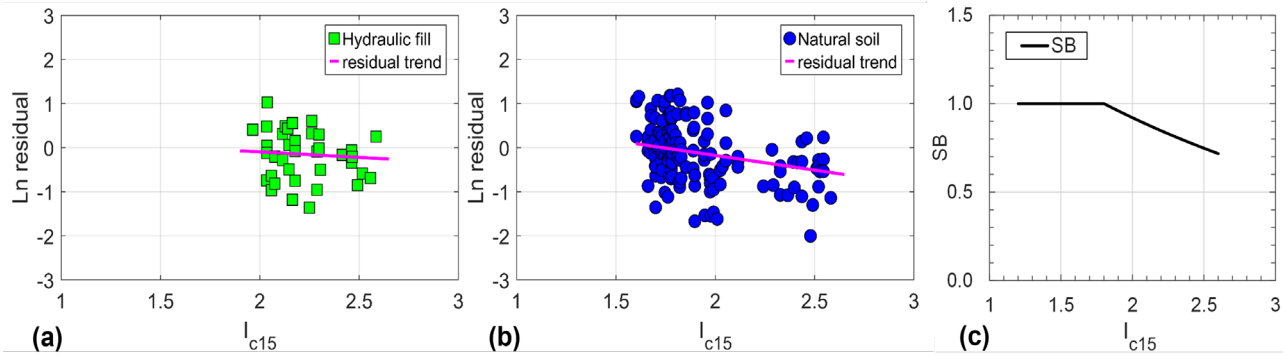

Figure 6.2. Residuals ($\ln(S_{v\_meas}) - \ln(S_{v\_est})$) vs. I_{c15} for: (a) hydraulic fill and (b) natural soil deposit, and (c) Soil Behavior factor relationship.

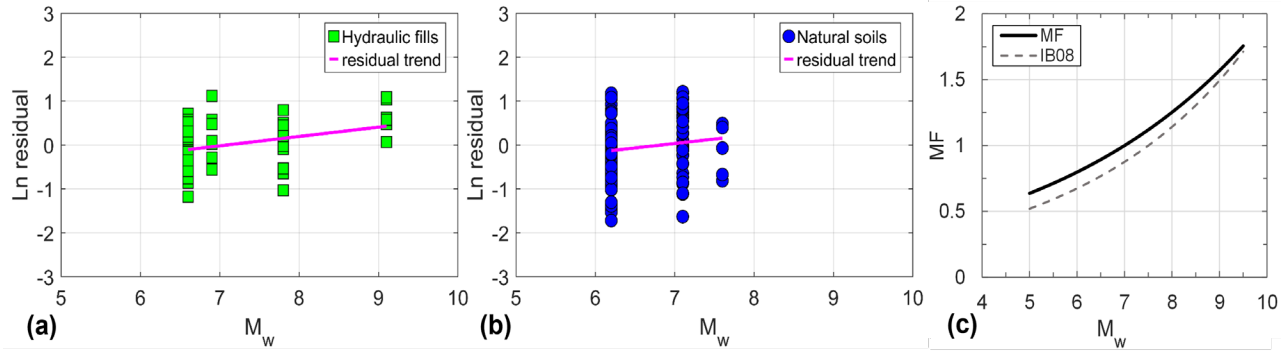

Figure 6.3. Residuals ($\ln(S_{v\_meas}) - \ln(S_{v\_est})$) vs. M_w for: (a) hydraulic fill and (b) natural soil deposit, and (c) Magnitude Factor relationship shown with Idriss and Boulanger (2008) *MSF*.

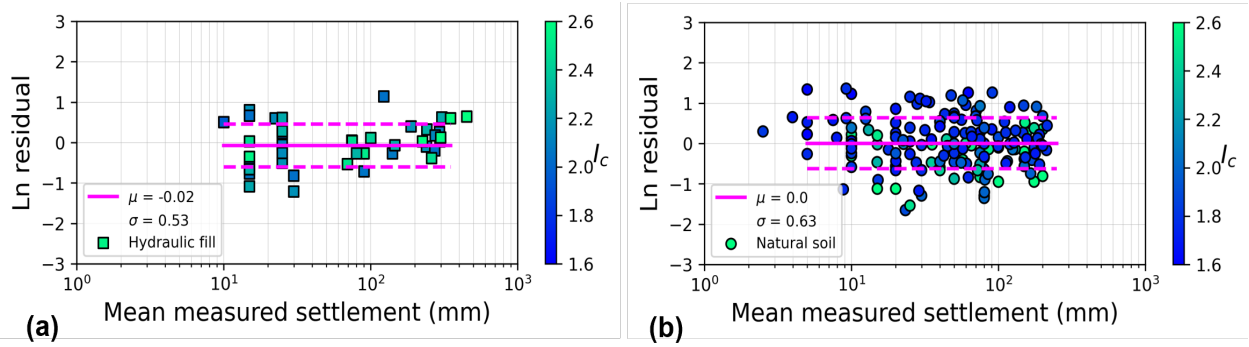

Figure 6.4. Proposed model residuals ($\ln(S_{v\_meas}) - \ln(S_{v\_est})$)for: (a) hydraulic fill and (b) natural soil deposit.

Chapter 7 CONCLUSION

7.1 Approach

Great challenges remain in geotechnical earthquake engineering. Professor H. Bolton Seed forged a path to advance knowledge in geotechnical earthquake engineering which can be followed. Throughout his career he integrated field case histories, laboratory experiments, and analyses in his studies. Analyses were not conducted to find the answer, but instead to gain insight. The authors employed Professor H. Bolton Seed's approach to evaluate liquefaction effects. Through examining field case histories, experiments, and analyses, insights are shared on the effects of liquefaction in the built environment.

7.2 Findings

Liquefaction-induced infrastructure settlement mechanisms are shear, volumetric, and ejecta. The problem is best viewed by examining soil response at the element level and soil deposit performance through its system response. The state of uniform clean sand, sandy gravel, nonplastic silty sand, and nonplastic silt can be examined in a unified manner using relative density and the state parameter. The cyclic responses of uniform fine sand, uniform nonplastic silty sand, and uniform coarse nonplastic silt are generally similar if at the same state and effective stress and loaded similarly. Post-liquefaction volumetric strain models are presented that capture this important soil response in a unified manner. In many cases, sandy gravels that are controlled by their sand matrix and clayey silts that respond similarly to nonplastic silts can be captured using models developed for sand, silty sand, and nonplastic silt.

The system response of a soil deposit often governs the consequences of liquefaction triggering. System response features affect greatly the formation of ejecta and its effects on infrastructure. Ejecta-induced settlement is challenging to estimate. However, through dynamic nonlinear effective stress analysis the importance of capturing the post-shaking hydraulic mechanisms that govern the upward flow of water was identified. The ejecta potential index indicates when ejecta are likely to occur and how extensive it would likely be when it occurs. A CPT-based method can be used to evaluate ejecta severity when there are insufficient resources to support effective stress analyses. Its liquefaction ejecta demand parameter L_D tends to increase systematically as ejecta severity increases at thick clean sand sites. Low L_D values are estimated at stratified soil sites that did not produce ejecta, which resolves the apparent overestimation by other liquefaction indices at stratified soil sites. The $L_D - C_R$ liquefaction ejecta severity chart separates cases with severe or extreme ejecta, which have high L_D and low C_R values, from cases with no ejecta, which have low L_D and high C_R values. The CPT-based liquefaction ejecta severity chart provides a preliminary estimate of the free-field, level ground ejecta-induced ground settlement.

The CPT should be the primary site investigation tool in most liquefaction evaluations. The CPT should be complemented with cyclic tests performed on high-quality samples when they are informative. The insights derived from cyclic tests support effective stress analyses which provides additional insights. However, there is no substitute for characterizing the depositional environment. Geologic details matter. Soil fabric is only indirectly assessed through most field and laboratory testing methods. Detailed logging of high-quality continuous samples to examine soil fabric and other important details should be performed when it is suspected that key factors will be missed using conventional sampling and in situ testing.

A probabilistic CPT-based post-liquefaction ground settlement procedure is proposed. It takes advantage of a recently compiled comprehensive laboratory database of post-liquefaction testing and a recently compiled comprehensive field case histories database of post-liquefaction settlement measurements. The volumetric strain of nonplastic soil with uniform gradation (SP, SM, and ML) can be estimated using D_r-based or ψ_o-based volumetric strain models. New correlations are developed to estimate D_r or ψ_o to enable use of the volumetric strain models. A calibration factor is required to adjust the estimates of natural soil deposits as these deposits have characteristics not well represented in the

laboratory tests used to develop the volumetric strain models. The calibration factor is not required for hydraulic fills. A soil behavior factor dependent on I_{c15} and a magnitude factor dependent on M_w are incorporated in the model to capture their effects on post-liquefaction ground settlement. The calibrated model captures the trends in the field measurements of post-liquefaction ground settlement well.

7.3 Future Research

Additional studies to develop alternative models and perspectives are warranted. The probabilistic CPT-based post-liquefaction level ground settlement procedure developed through this study can be combined with CPT-based shear-induced settlement and ejecta-induced settlement procedures to estimate the total settlement of buildings and to make preliminary estimates of the total settlement of bridges. Additional experimental and numerical studies are required to integrate these approaches for specific engineering applications, such as bridges, because the research performed currently has focused on liquefaction-induced settlement of level ground and of buildings founded on level ground sites. As stated previously, great challenges remain in geotechnical earthquake engineering, especially in the evaluation of liquefaction effects on structures. Liquefaction research can advance the state-of-the-art by focusing on understanding and evaluating the effects of liquefaction on bridges and buildings and developing innovative mitigation methodologies.

REFERENCES

Akai et al. (1995). Geotechnical reconnaissance of the effects of the January 17, 1995, Hyogoken-Nanbu Earthquake, Japan. Sitar, N., ed., Earthquake Engineering Research Center, Report No. UCB/EERC-95/01, Univ. of California, Berkeley, July.

Baker J.W., Cornell, C.A. (2006). Correlation of response spectral values for multi-component ground motions. *Bull. Seismol. Soc. Am*. 96, 215–227

Been, K. and Jefferies, M.G. (1985). A state parameter for sands. *Geotechnique,* 35(2), 99-112.

Beyzaei, C. Z. (2017). Fine-grained soil liquefaction effects in Christchurch, New Zealand. *Ph.D. Dissertation*. Berkeley, Univ. of California, Berkeley, CA.

Beyzaei, C.Z., Bray, J.D., van Ballegooy, S., Cubrinovski, S., and Bastin, S. (2018a) "Depositional environment effects on observed liquefaction performance in silt swamps during the Canterbury earthquake sequence," *Soil Dynamics and Earthquake Engineering* J., 107, 303-321.

Beyzaei, C.Z., Bray JD, Cubrinovski M, Riemer M, Stringer M. (2018b). Laboratory-based characterization of shallow silty soils in southwest Christchurch. *Soil Dyn. Earthquake Eng*, 110, 93–109.

Beyzaei, C.Z., Bray, J.D., Cubrinovski, S., Bastin, S., Riemer, M., Stringer, M., Jacka, M., van Ballegooy, S., and Wentz, R. (2020) "Characterization of silty soil thin-layering and groundwater conditions for liquefaction assessment," *Canadian Geotechnical J.*, doi: 10.1139/cgj-2018-0287.

Bilge, H.T. (2010). Cyclic volumetric and shear strain response of fine-grained soils. *Ph.D. Dissertation*. Turkey, Middle East Technical University.

Bolton, M.D. (1986). The strength and dilatancy of sands. *Geotechnique,* 36(1), 65-78.

Boulanger, R.W., Idriss, I.M. (2008). Closure to "Evaluation of cyclic softening in silts and clays" by Ross W. Boulanger and I. M. Idriss. *J. Geotech. Geoenviron. Eng*., ASCE, 135(2), 308.

Boulanger R.W., Idriss I.M. (2016). CPT-based liquefaction triggering procedures. *J Geotech Geoenviron Eng*., ASCE, 142(2), 04015065.

Bray J.D., Macedo J. (2017). 6th Ishihara lecture: Simplified procedure for estimating liquefaction-induced building settlement. *Soil Dynam Earthq Eng* 017, 102, 215–31.

Bray, J. D., R. B. Sancio, H.T. Durgunoglu, A. Onalp, T. L. Youd, J. P. Stewart, R. B. Seed, O.K. Cetin, E. Bol, M. B. Baturay, C. Christensen, and T. Karadayilar. (2004). Subsurface characterization at ground failure Sites in Adapazari, Turkey. *J. Geotech. Geoenviron. Eng.* , ASCE, V.130(7), 673-685.

Bray, J. D. and Sancio, R. B. (2006). Assessment of the liquefaction susceptibility of fine-grained soils. *J. Geotech. Geoenviron. Eng*., ASCE, 132(9), 1165–1177.

Bray, J. D. and Sancio, R. B. (2008). Closure to "Assessment of the liquefaction susceptibility of fine-grained soils" by Jonathan D. Bray and Rodolfo B. Sancio. *J. Geotech. Geoenviron. Eng*., ASCE, 134(7), 1031–1034.

Bray, J.D., Cubrinovski, M., Zupan, J., and Taylor, M. (2014a). Liquefaction effects on buildings in the Central Business District of Christchurch. *Earthquake Spectra J.*, EERI, V. 30(1), 85-109, doi: 10.1193/022113EQS043M.

Bray, J.D., Cubrinovski, M., Zupan, J., Taylor, M., (2014b). CPT-based liquefaction assessments in Christchurch, New Zealand. In: *Proc. CPT'14: Third International Symposium on Cone Penetration Testing*. Las Vegas, NV, May 13–14.

Bray, J.D., Boulanger, R.W., Cubrinovski, M, Tokimatsu, K., Kramer, S.L., O'Rourke, T., Rathje, E., Green, R.A., Robertson, P., and Beyzaei, C.S. (2017). U.S.–New Zealand–Japan International Workshop, Liquefaction-induced ground movements effects, *2–4 November 2016 PEER Report 2017/02*, University of California, Berkeley, California.

Bullock, Z., Karimi, Z., Dashti, S., Porter, K., Liel, A.B., Franke W. (2019). A physics-informed semi-empirical probabilistic model for the settlement of shallow-founded structures on liquefiable ground. *Géotechnique* 69(5), 406-419

Cetin K.O., Bilge H.T., Wu J., Kammerer A.M., Seed R.B. (2009). Probabilistic models for cyclic

straining of saturated clean sands. *J Geotech Geoenviron Eng*, 135(3), 71–86.
Chin, R. (1987). Volumetric strain characteristics of saturated sand under cyclic loadings. *Proc. 9th Southeast Asian Geotechnical Conference*, Bangkok, Thailand, 7.81-7.90
Cubrinovski, M., Bray, J.D., Taylor, M., Giorgini, S., Bradley, B., Wotherspoon, L., and Zupan, J. 2011. Soil liquefaction effects in the central business district during the February 2011 Christchurch Earthquake. *Seismological Research Letters*, V. 82(6), 893-904.
Cubrinovski, M., Rhodes, A., Ntritsos, N., and van Ballegooy, S. (2018a). System response of liquefiable deposits. *Soil Dyn. Earthquake Eng,* https://doi.org/10.1016/j.soildyn.2018.05.013.
Cubrinovski, M., Bray, J.D., de la Torre, C., Olsen, M., Bradley, B.A., Chiaro, G., Stocks, E., Wotherspoon, L., and Krall, T. (2018b). Liquefaction-induced damage and CPT characterization of the reclamations at CentrePort, Wellington. *B. Seismological Society of America*, V. 108(3).
Cubrinovski M. (2019). Some important considerations in the engineering assessment of soil liquefaction. *New Zealand Geomechanics News*. 97.
Cubrinovski M, and Ishihara K. (2002). Maximum and minimum void ratio characteristics of sands. *Soils Found*., 42(6), 65–78.
Dhakal, R., Cubrinovski, M., and Bray, J.D. (2020). Geotechnical characterization and liquefaction evaluation of gravelly reclamations and hydraulic fills (Port of Wellington, New Zealand). *Soils and Foundations*, V. 60, 1507-1531, https://doi.org/10.1016/j.sandf.2020.10.001.
Dhakal, R., Cubrinovski, M., and Bray, J.D. (2022). Evaluating the applicability of conventional CPT-based liquefaction assessment procedures to reclaimed gravelly soils. *Soil Dyn. Earthquake Eng.* 155, 107176
Dobry, R. and Ladd, R. (1980). Discussion on "Soil liquefaction and cyclic mobility evaluation for level ground during earthquakes and liquefaction potential: science versus practice". *ASCE J Geotech Eng Div*, 106, 720–724.
Donahue, J.L., Bray, J.D., and Riemer, M.F. (2007). Liquefaction Testing of Fine-Grained Soil Prepared Using Slurry Deposition," Proc. 4th Inter. Conf. Earthquake Geotechnical Engineering, Paper No. 1226.
Duku, P.M., Stewart, P.M., Whang, D.H., and Yee, E. (2008). Volumetric strains of clean sands subject to cyclic loads. *ASCE J Geotech Eng Div*, 134(8), 1073–1078.
Duncan, J. M., Wright, S. G., Brandon, T. L. (2014). Soil strength and slope stability. *Germany: Wiley*.
ENGEO (2016). Dynamic behavior of the Treasure Island natural shoal deposit. Sam Francisco, CA, Report No. 7091.000.000-T4, March 18.
Hutabarat, D., and Bray J.D. (2021a). Effective stress analysis of liquefiable sites to estimate the severity of sediment ejecta. *ASCE J Geotech Eng Div* , ASCE, V. 147(5).
Hutabarat, D., and Bray J.D. (2021b). Seismic response characteristics of liquefiable sites with and without sediment ejecta manifestation. *ASCE J Geotech Eng Div* , ASCE, V. 147(6).
Hutabarat, D., and Bray J.D. (2022). Estimating the severity of liquefaction ejecta using the Cone Penetration Test. *ASCE J Geotech Eng Div* , ASCE, V. 148(3).
Idriss I, Boulanger R. (2008). Soil liquefaction during earthquakes. *Earthquake Engineering Research Institute (EERI)*, MNO-12.
Ishihara, K. (1993) Liquefaction and flow failure during earthquakes. *Géotechnique*, 43, 351-415.
Ishihara K, and Yoshimine M. (1992). Evaluation of settlements in sand deposits following liquefaction during earthquakes. *Soils Found*., 32(1),173–188.
Iwasaki, T., F. Tatsuoka, K. Tokida, and S. Yasuda. 1978. "A practical method for assessing soil liquefaction potential based on case studies at various sites in Japan." *In Proc., 2nd Int. Earthquake Microzonation Conf*., 885–896. Washington, DC: National Science Foundation.
Jefferies, M., and Been, K. (2016). Soil liquefaction: A critical state approach, 2nd edition. *Florida: Taylor & Francis Group*.
Japanese Geotechnical Society. (2000). JIS A 1224:2000 - Test methods for minimum and maximum densities of sands, *Soil Testing Standards*; 136-138 (In Japanese).
Ku C.S., Juang, C. H., Chang, C. W., and Ching J. (2012). Probabilistic version of the Robertson and

Wride method for liquefaction evaluation: development and application. *Canadian Geotechnical J.*, 49(1), 27-44
Ladd, R.S. (1977). Specimen preparation and cyclic stability of sands. *J. Geotech. Eng. Division*. 103, GT6, 535-547.
Lee, K. L., and Albaisa, A. (1974). Earthquake induced settlements in saturated sands. *J. Geotech. Eng. Division*. GT4, 387-406.
Luque, R, and Bray, J.D. (2017). Dynamic analyses of two buildings founded on liquefiable soils during the Canterbury earthquake sequence. *J Geotech Geoenviron Eng*. 143(9), 04017067, 1-14
Markham, C. S. (2015). Response of liquefiable sites in the Central Business District of Christchurch, New Zealand, *Ph.D. Dissertation*. Berkeley, Univ. of California.
Markham, C.S., Bray, J.D., Riemer, M.F, and Cubrinovski, M. (2016). Characterization of shallow soils in the central business district of Christchurch, New Zealand. *Geotechnical Testing J*., ASTM, doi:10.1520/GTJ2015024.
Markham, C.S., Bray, J.D., Cubrinovski, M. and Riemer, M. (2018). Liquefaction resistance and steady-state characterization of shallow soils within the Christchurch Central Business District. *ASCE J Geotech Geoenviron Eng*, 144(6), 04018032.
Mayne, P.W. and Styler, M. (2018). Soil liquefaction screening using CPT yield stress profiles. *Proc. Geotech Earthq Eng Soil Dyn V*, Austin, Texas, 605-616.
Mijic, Z., Bray, J.D., Riemer, M.F., Cubrinovski, M., and Rees, S.D. (2021a). Test method for minimum and maximum densities of small quantities of soil. *Soils Found*, 61(2), 533–540.
Mijic, Z., Bray, J.D., Riemer, M.F., Rees, S.D., and Cubrinovski M. (2021b). Cyclic and monotonic simple shear testing of native Christchurch silty soil, *Soil Dyn. Earthquake Eng*, 148.
Mijic, Z, Bray, J.D., and van Ballegooy, S. (2022). Liquefaction Ejecta Case Histories for 2010-11 Canterbury Earthquakes. *International Journal of Geoengineering Case Histories*, ISSMGE, in press.
Mitchell, J. and Soga, K. (2005). Fundamentals of soil behavior, 3rd edition. *John Wiley & Sons*, Hoboken.
Mulilis, J.P., Seed, H.B., Chan, C.K., Mitchell, J.K., and Arulanandan, K. (1977). Effects of sample preparation on sand liquefaction. ASCE Journal of the Geotechnical Engineering Division. 103, GT2, 91-108.
Olaya F.R., and Bray J.D. (2022a). CPT case histories of post-liquefaction free-field ground settlement. *J Geotech Geoenviron Eng*., *11 July 2022 Geosystems Engineering Report UCB/GT 2022-02*, Univ. of California, Berkeley.
Olaya F.R., and Bray J.D. (2022b). Strain potential of liquefied soil. *J Geotech Geoenviron Eng*., 148(11), doi: 10.1061/(ASCE)GT.1943-5606.0002896.
Polito, C. P., and Martin, J. R., II. (2001). "Effects of nonplastic fines on the liquefaction resistance of sands." *J. Geotech. Geoenviron. Eng*., 127(5), 408–415.
Robertson P.K. (2009). Performance-based earthquake design using the CPT. *International Conference on Performance-Based Design in Earthquake Geotechnical Engineering* (Is-Tokyo 2009).
Robertson, P.K. (2010). Estimating in-situ state parameter and friction angle in sandy soils from CPT. *2nd International Symposium on cone Penetration Testing*.
Robertson, P.K. (2016). Cone Penetration Test (CPT)-based soil behaviour type (SBT) classification system – an Update. *Can Geotech J*, 00, 1–18.
Robertson P.K., and Cabal K.L. (2015). Guide to CPT for geotechnical engineering, 6th ed., *Gregg Drilling Testing, Inc*. Signal Hill, CA.
Robertson P.K., and Wride C.E. (1998). Evaluating cyclic liquefaction potential using the Cone Penetration Test, *Can. Geotech. J*., 35(3):442–459.
Roscoe, K.H., Schofield, A. N., and Wroth C.P. (1958). On the yielding of soils. *Geotechnique*; 8, 22-53
Russell, J., and van Ballegooy, S. (2015). Canterbury earthquake sequence: increased liquefaction vulnerability assessment methodology. *T+T Report 0028-1-R-JICR-2015 prepared for the Earthquake Commission.*
Seed, H.B. (1979). Soil liquefaction and cyclic mobility evaluation for level ground during earthquakes. *J.*

Geotech. Eng. Division. GT2, 201-255.
Shuttle, D.A. and Cunning J. (2007). Liquefaction potential of silts from CPTu. *Can Geotech J,* 45, 140–141.
Shuttle, D.A. and Cunning J. (2008). Reply to the discussion by Robertson on "Liquefaction Potential of Silts from CPTu". *Can Geotech J*, 45,142–145.
Tatsuoka, F., Zhou, S., Sato, T., and Shibuya, S. (1990). Method of evaluating liquefaction potential and its application. In Report on seismic hazards on the ground in urban areas, Ministry of Education of Japan, Tokyo. (in Japanese.)
Thevanayagam S, Shenthan T, Mohan S, and Liang J. (2002). Undrained fragility of clean sands, silty sands, and sandy silts. *ASCE J Geotech Geoenviron Eng,* 128(10), 849–859.
Toriihara, M., Yamada,Y., Morimoto, I. and Ishihara, K. (2000). The characteristics of settlement after liquefaction for sand containing fines, *Proc 35th Japan Conference on Geotechnical Engineering*, 3, 1655-1656. (In Japanese).
van Ballegooy, S., F. Wentz, and R. W. Boulanger. (2014). Evaluation of CPT-based liquefaction procedures at regional scale." *Soil Dyn. Earthquake Eng*. 79 315–334.
Whang, D. H. (2001). Seismic compression of compacted soils, *Ph.D. Dissertation*. Los Angeles: Univ. of California.
Yasuda S., Ishihara K., Harada K., and Shinkawa, N. (1996). Effect of soil improvement on ground subsidence due to liquefaction. *Soils Found*, Special Issue, 99-107.
Yoshimine, M., Nishizaki, H., Amano, K., and Hosono, Y. (2006). Flow deformation of liquefied sand under constant shear load and its applications to analysis of flow slide in infinite slope. *Soil Dyn. Earthquake Eng*, 26, 253–264.
Youd, T., and Perkins, D. (1978). Mapping liquefaction-induced ground failure potential. *J. Geotech. Eng. Division*. GT4, 433-446.
Zhang G., Robertson P.K., and Brachman R.W.I. (2002). Estimating liquefaction-induced ground settlements from CPT for level ground. *Can Geotech J*, 39, 1168–1180.
Zhang G., Robertson P.K., and Brachman R.W.I. (2004). Estimating liquefaction induced lateral deformations from SPT and CPT, *ASCE. J Geotech Geoenviron Eng*. 130(8). 861–871.